

NASA/TM—2014-218389



Development and Testing of an ISRU Soil Mechanics Vacuum Test Facility

Julie E. Kleinhenz
Glenn Research Center, Cleveland, Ohio

R. Allen Wilkinson
National Center for Space Exploration Research, Cleveland, Ohio

NASA STI Program . . . in Profile

Since its founding, NASA has been dedicated to the advancement of aeronautics and space science. The NASA Scientific and Technical Information (STI) program plays a key part in helping NASA maintain this important role.

The NASA STI Program operates under the auspices of the Agency Chief Information Officer. It collects, organizes, provides for archiving, and disseminates NASA's STI. The NASA STI program provides access to the NASA Aeronautics and Space Database and its public interface, the NASA Technical Reports Server, thus providing one of the largest collections of aeronautical and space science STI in the world. Results are published in both non-NASA channels and by NASA in the NASA STI Report Series, which includes the following report types:

- **TECHNICAL PUBLICATION.** Reports of completed research or a major significant phase of research that present the results of NASA programs and include extensive data or theoretical analysis. Includes compilations of significant scientific and technical data and information deemed to be of continuing reference value. NASA counterpart of peer-reviewed formal professional papers but has less stringent limitations on manuscript length and extent of graphic presentations.
- **TECHNICAL MEMORANDUM.** Scientific and technical findings that are preliminary or of specialized interest, e.g., quick release reports, working papers, and bibliographies that contain minimal annotation. Does not contain extensive analysis.
- **CONTRACTOR REPORT.** Scientific and technical findings by NASA-sponsored contractors and grantees.

- **CONFERENCE PUBLICATION.** Collected papers from scientific and technical conferences, symposia, seminars, or other meetings sponsored or cosponsored by NASA.
- **SPECIAL PUBLICATION.** Scientific, technical, or historical information from NASA programs, projects, and missions, often concerned with subjects having substantial public interest.
- **TECHNICAL TRANSLATION.** English-language translations of foreign scientific and technical material pertinent to NASA's mission.

Specialized services also include creating custom thesauri, building customized databases, organizing and publishing research results.

For more information about the NASA STI program, see the following:

- Access the NASA STI program home page at <http://www.sti.nasa.gov>
- E-mail your question to help@sti.nasa.gov
- Fax your question to the NASA STI Information Desk at 443-757-5803
- Phone the NASA STI Information Desk at 443-757-5802
- Write to:
STI Information Desk
NASA Center for AeroSpace Information
7115 Standard Drive
Hanover, MD 21076-1320



Development and Testing of an ISRU Soil Mechanics Vacuum Test Facility

*Julie E. Kleinhenz
Glenn Research Center, Cleveland, Ohio*

*R. Allen Wilkinson
National Center for Space Exploration Research, Cleveland, Ohio*

National Aeronautics and
Space Administration

Glenn Research Center
Cleveland, Ohio 44135

Trade names and trademarks are used in this report for identification only. Their usage does not constitute an official endorsement, either expressed or implied, by the National Aeronautics and Space Administration.

Level of Review: This material has been technically reviewed by technical management.

Available from

NASA Center for Aerospace Information
7115 Standard Drive
Hanover, MD 21076-1320

National Technical Information Service
5301 Shawnee Road
Alexandria, VA 22312

Available electronically at <http://www.sti.nasa.gov>

Development and Testing of an ISRU Soil Mechanics Vacuum Test Facility

Julie E. Kleinhenz
National Aeronautics and Space Administration
Glenn Research Center
Cleveland, Ohio 44135

R. Allen Wilkinson
National Center for Space Exploration Research
Cleveland, Ohio 44135

Abstract

For extraterrestrial missions, earth based testing in relevant environments is key to successful hardware development. This is true for both early component level development and system level integration. For In-Situ Resource Utilization (ISRU) on the moon, hardware must interface with the surface material, or regolith, in a vacuum environment. A relevant test environment will therefore involve a vacuum chamber with a controlled, properly conditioned bed of lunar regolith simulant. However, in earth-based granular media, such as lunar regolith simulant, gases trapped within the material pore structures and water adsorbed to all particle surfaces will release when exposed to vacuum. Early vacuum testing has shown that this gas release can occur violently, which loosens and weakens the simulant, altering the consolidation state.

A mid-size chamber (3.66 m tall, 1.5 m inner diameter) at the NASA Glenn Research Center has been modified to create a soil mechanics test facility. A 0.64 m deep by 0.914 m square metric ton bed of lunar simulant was placed under vacuum using a variety of pumping techniques. Both GRC-3 and LHT-3M simulant types were used. Data obtained from an electric cone penetrometer can be used to determine strength properties at vacuum including: cohesion, friction angle, bulk density and shear modulus. Simulant disruptions, caused by off-gassing, affected the strength properties, but could be mitigated by reducing pump rate. No disruptions were observed at pressures below 2.5 Torr, regardless of the pump rate. The slow off-gassing of the soil at low pressure lead to long test times; a full week to reach 10^{-5} Torr. Robotic soil manipulation would enable multiple ISRU hardware test within the same vacuum cycle. The feasibility of a robotically controlled auger and tamper was explored at vacuum conditions.

Nomenclature

CP	Cone Penetrometer
CPT	Cone Penetrometer Test
dP/dt	Change in pressure with respect to time
GRC	Glenn Research Center
ISRU	In-Situ Resource Utilization
LN2	Liquid Nitrogen
LHT	Lunar Highlands Type
RGA	Residual Gas Analyzer
VF	Vacuum Facility

1.0 Introduction

Future exploration efforts will require use of in-situ resources to effectively sustain our presence off-earth. By producing consumables like water and oxygen from the soil, it is possible to reduce the dependence on earth for resupply. In this manner, In-Situ Resource Utilization (ISRU) can reduce mission cost and risk (Ref. 1).

ISRU systems can consist of various hardware and processes such as excavation, traction, material handling, drilling operations, and chemical reaction of the soil. As these different types of subsystems advance and begin to integrate into larger systems, there is an increasing need for realistic test beds. For application to a lunar mission, an integrated test bed will require a soil bed (using lunar regolith simulants) in a vacuum chamber, amongst other environmental controls like temperature and radiation. The depth profile (density, bearing strength, shear strength, layering) of the soil bed must mimic the lunar surface and sub-surface with fidelity.

The effect of gas pressure on a soil state, however, is not fully characterized, though a variety of related tests have been performed (Refs. 2 to 12). The always present void space in dry soils contains gas that seeks to be of an equal pressure to the ambient outside the soil. The water and passivation layers on soil particles also affect inter-particle friction and adhesion. The pressure environment, and/or the pump down process, may influence the soil state. Previous experiments with small samples of lunar regolith simulant in a vacuum demonstrated an energetic release of trapped gases as the simulant was exposed to vacuum (Ref. 13). This would cause mixing or ‘fluffing’ of the simulant and change the consolidation state, thus ruining pre-preparation of the soil bed. While extensive drying and pre-preparation of the simulant may mitigate these off-gas disruptions, this is impractical for ISRU component testing which can require on the order of 1000 kg of simulant.

The Vacuum Facility #13 (VF13), a mid-size chamber at the NASA Glenn Research Center, has been modified to create a soil mechanics test facility to study these effects (Fig. 1). Using a 1 ton bin of lunar regolith simulant, tests were performed to explore the simulant behavior at reduced pressure. A cone penetrometer was used to measure consolidation state before, during, and after vacuum exposure. A residual gas analyzer (RGA) was used during vacuum pump down to determine off-gassed constituents. The distributions caused by gas release were examined and mitigation techniques identified. Slow off-gassing of the simulant, even with no disturbances, lead to long vacuum pump down times. Thus, ways of conditioning the soil while under vacuum were explored so that the appropriate consolidation state could be generated in-situ. This included a tamper for compaction and a cork-screw auger for tilling.



Figure 1.—Photo of the vacuum facility (A) with the lid and (B) without the lid, showing the research hardware. The tall structure is the cone penetrometer.

<u>Phase 1</u>	<u>Phase 2</u>
<ul style="list-style-type: none"> • Examine simulant/pressure interaction <ul style="list-style-type: none"> – No soil manipulation • Facility checkout and improvements <ul style="list-style-type: none"> – Hardware performance – Soil contamination • Obtain baseline CPT data at vacuum 	<ul style="list-style-type: none"> • Manipulate soil at vacuum to obtain desired consolidation state <ul style="list-style-type: none"> – Compaction – Tilling • Enact facility improvements to increase vacuum efficiency • Obtain CPT data before/during/after vacuum. <ul style="list-style-type: none"> – Multiple penetrations

Figure 2.—Summary of the two phases of testing. Note the CPT is Cone Penetrometer Test.

Since this is the first soil mechanics test facility of its size, one of the critical functions of this test program was to learn about the logistics and operations of a large scale dirty vacuum chamber. The techniques and operation methods will feed into operation and buildup of full scale facilities that will be needed for full systems testing. Meanwhile, the VF13 facility is actively available as a (sub-) systems test facility. Following this report, VF13 was modified with a removable cold wall to achieve cryogenic thermal-vacuum conditions.

A total of five tests were performed in VF13. Three tests were performed during the phase 1 portion of the project, which was intended to explore operational logistics of the facility and develop test procedures (Ref. 14). Baseline cone penetration data was also gathered at vacuum conditions. In the two tests of phase 2, robotic soil manipulation hardware was added: a tamper for soil compaction and an auger for tilling. These, along with the penetrometer, were mounted on a 2-D translation stage so the entire soil surface could be accessed. A summary of the two phases is shown in Figure 2. The first two tests utilized GRC-3 lunar soil simulant (Ref. 15) (a sand and silt mix), while all others used LHT-3M a higher fidelity lunar highlands regolith simulant (Ref. 16). The “-3M” indicates it lacks the agglutinates and trace minerals found in “-2M”.

2.0 Facility

The Vacuum Facility #13 (VF13) at the NASA Glenn Research Center was modified into a mid-size soil mechanics test facility. It is a vertical, cylindrical chamber 3.66 m tall with an internal volume of 6.35 m³ (Fig. 1(A)). The bulk of the volume is within the removable 2.52 m tall by 1.5 m diameter lid. The fixed base is 1.08 m deep and accommodates a variety of electrical, mechanical, and gas feed-throughs. The dimensions of this chamber, namely the height, were well suited for a sufficiently deep soil bin along with vertically oriented hardware, such as the cone penetrometer or a drill. The several vacuum pumps on the facility allowed a well-controlled pressure decay rate for all stages of operations. After this test program completed, VF13 was further modified to support an internal cold wall, or thermal shroud, to provide cryogenic temperature conditions within the chamber.

2.1 Vacuum Pumps: Types and Operation Notes

The facility is capable of achieving pressures in the 10⁻⁶ Torr range or below. While this does not constitute an “ultra-high vacuum” of the lunar surface (10⁻¹² Torr scale, Ref. 18), it is believed to be sufficient to examine macro scale simulant interactions. This is also an economical vacuum range given the cost associated with high vacuum chambers of this size. A variety of vacuum pumps were used to achieve the target operating pressure for these tests (Table 1). These included a venturi pump, a roughing pump (brand name “Kinney”), a turbo molecular (or “turbo”) pump, and a cryogenic (or “cryo”) pump.

TABLE 1.—VACUUM PUMP CAPABILITY SUMMARY

	Venturi	Kinney	Turbo	Cryo
Operational pressure range, Torr	760 to 30	760 to 0.1 (no load) 760 to 1 (loaded)	0.75 to 10 ⁻⁶	0.1 to 10 ⁻⁶
Advantages	Tolerant to all contaminants. Slow pressure decay prevented soil disturbance. Safe for unattended operation.	Permitted throttled pump down through, 10 ⁻¹ Torr which is stage at which soil disturbance was most likely.	Tolerant to water off-gassing. Excellent pump of low atomic weight gasses. Safe for unattended operation.	Large pumping rate. Dirt tolerant. Excellent pump for water and heavier molecules. Can regenerate pump without affecting vacuum in main chamber.
Limitations	Limited pressure range	Possible contamination of pump oil from particulates or water	Particulate contamination and vibration pose a hazard to high speed turbine.	Requires periodic shutdown when cold surface saturates with condensed gases (water) or particulates
			Under heavy loading, may hit temperature auto-shut off limit of 75 °C. Additional cooling is required down to 10 ⁻³ Torr	Pump start up takes 4 hr Regeneration of cold surface takes an additional 4 to 6 hr
			De-activated during soil manipulation to prevent contamination issues	

The slow off-gassing of the regolith simulant lead to long pump down times. This heavier gas load on the pumps also affected their behavior and efficiency. The sections below detail the operation of each pump, along with some issues encountered.

2.1.1 Baseline Pressure Test

Figure 3 shows the baseline pressure profile of the facility during pump down. For this test, the chamber was empty; no regolith simulant or hardware was present. This profile will be used in later sections to compare the effect of soil off-gassing on pressure decay rates and performance. The active pumps at any given time are listed at the top of the figure. Note that the sequence of pump activation, particularly the turbo and cyro pumps, was governed by the maximum operating pressures of the pumps. This will be discussed in the following sections. The pressure decline generally followed an asymptotic profile, with the pumps becoming less effective at lower pressures.

At the end of this test, all pumps were isolated and deactivated. The chamber was left in this condition over one weekend (~64 hr) to examine pressure rise and verify seal integrity. The results are shown in Figure 4. The main graph shows the pressure rise in log scale to resolve the detail while the inset graph shows the same data in linear scale. There is a rapid rise during the first several hours, then levels off, possibly approaching an asymptote. This rate will be dependent on pressure, decaying as it approaches pressure equilibrium. Thus, the power fit (green dash line) is a more accurate description of this behavior. However, the linear fit (red line) can be used as an approximation, where the slope term is a simple pressure ‘leak’ rate. Using this approximation, the pressure rise during the more ‘steady’ portion of the run (starting at 0.03 Torr, at the 10 hr mark) is 3.87×10⁻³ Torr/hour. A slight deformation in the sealing flange was noticed during the test program, along with scuffing of the chamber’s main O-ring, which likely accounts for the unusual leakage. These are being addressed.

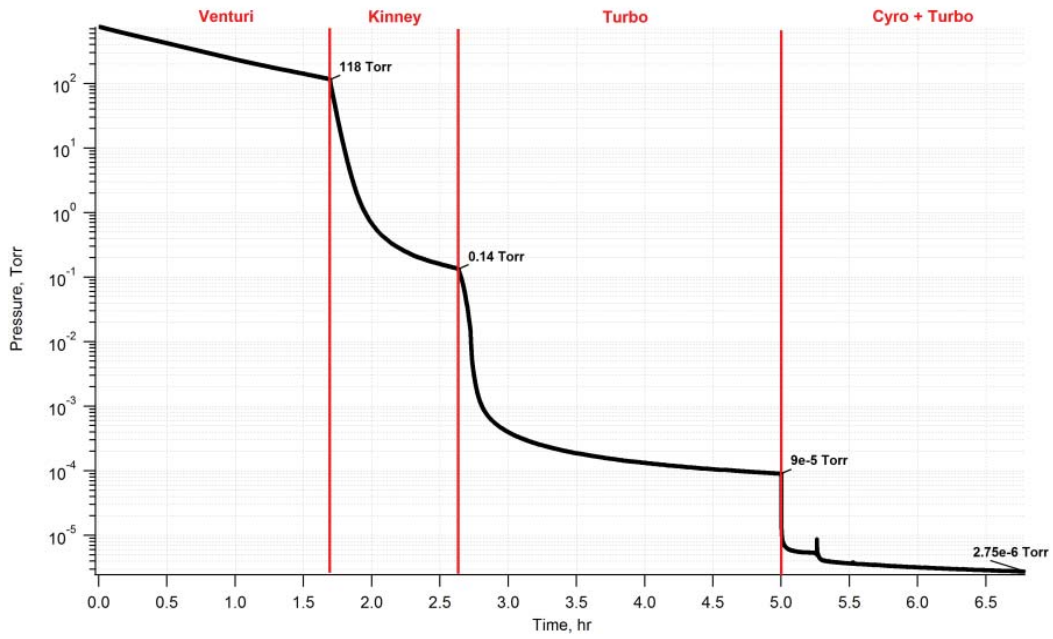


Figure 3.—Baseline pressure test with no hardware or soil in the chamber.

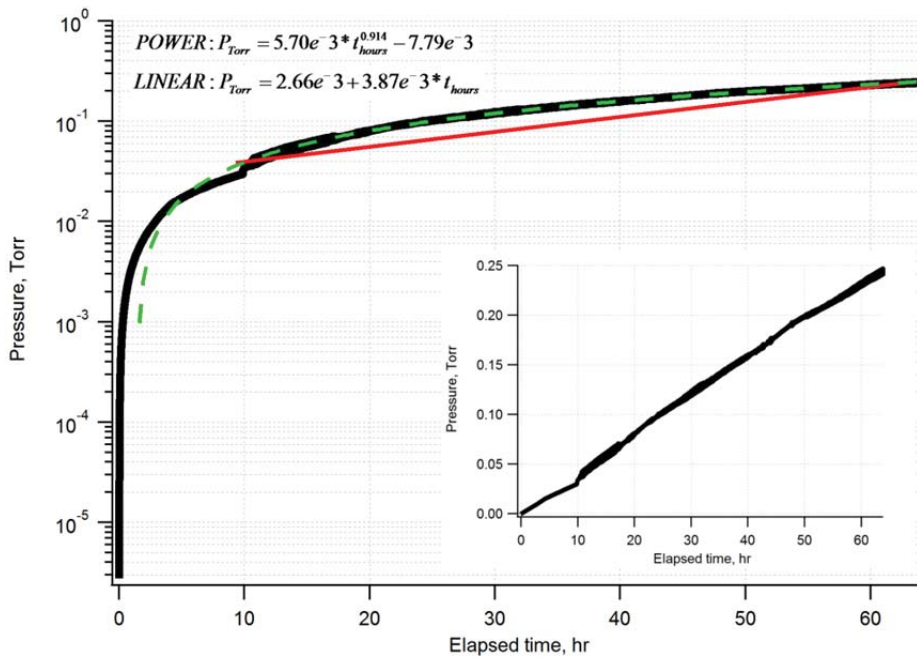


Figure 4.—Pressure rise after vacuum pump deactivation.



Figure 5.—The venturi pump on VF13.

2.1.2 Venturi Pump

As the name indicates, the venturi pump (Fig. 5) operates on the venturi effect. Compressed gaseous nitrogen flows through an orifice resulting in a pressure decrease. This pump has no moving parts and is insensitive to potential contamination from the regolith simulant particles. However, its effective range is limited: 760 to 30 Torr. Once 30 Torr is reached (after 4.5 hr starting at atmospheric pressure), there is no further decline, pressure holds constant. In this test series, the pressure decay rate over this range was very consistent and predictable.

During testing with the simulant bed, this pump was the first activated. While a displacement type “roughing pump” is traditionally used at room conditions, the soil bed was more susceptible to off-gassing soil disturbances at this pressure range. The airborne particulates from these disturbances could contaminate the roughing pump oil, but posed no contamination risk to the venturi pump. Thus the venturi pump was ideal for initial ‘rough’ pump down. The pressure decay rate of the venturi pump is also slower than traditional roughing pumps which also helped mitigate soil disturbances altogether.

2.1.3 Roughing (Kinney) Pump

The term “roughing” pump generally refers to a pump used in the first stage of pump down, starting at atmospheric pressure. The facility’s traditional roughing pump is a “Kinney” brand rotary piston pump. The piston drives an eccentrically mounted cylinder around the pump cavity. The gas is compressed as the cam rotation reduces the volume. For the baseline (empty chamber) test, the pump’s performance began to fall off in the 10^{-1} Torr range, but with the soil load present, the pump was undesirably slow below 1 Torr.

While rotary pumps tend to be rugged, they do require oil lubricant. Thus contamination from soil particulates is a concern. During the first soil test (test 1) the Kinney pump seized. This was initially attributed to soil contamination, but post-analysis of the oil did not reveal appreciable particulate matter. The failure was later attributed to a preexisting flaw in the pump itself. However, steps were taken to protect the pump from contamination for the remainder of the test series. A multi-trap filter element (Fig. 6) was added to the pump inlet. This contained a series of four filter elements as well a cooling coil to capture condensable gases, such as water. A 1.8 m tall inverted u-tube (Fig. 6) was also installed on the chamber port to encourage particulate elutriation. A non-immersion oil trap was located at the downstream end of the tube to capture any remaining particles (the linear momentum particles traveling down the tube impinged the oil surface before they could turn the corner into the pump). Inspection of the filters and the oil traps post-test showed very little particle accumulation.

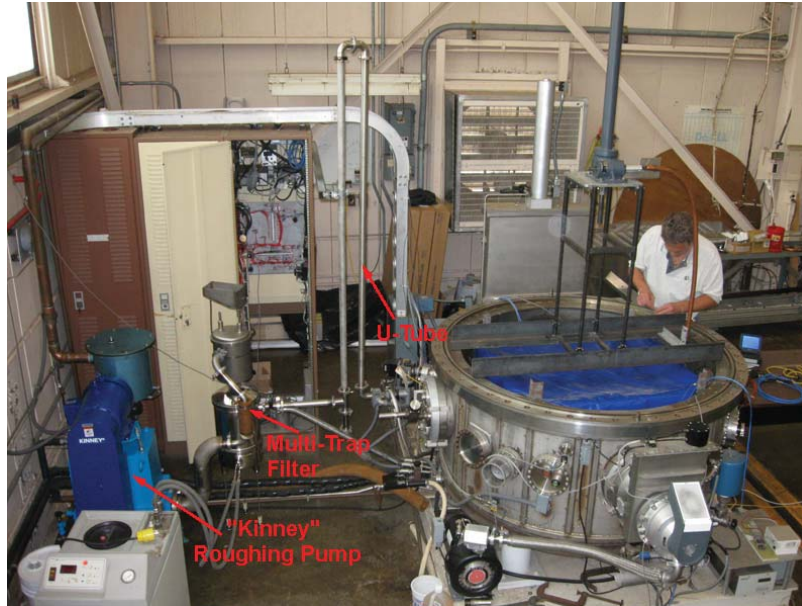


Figure 6.—The Kinney roughing pump with the inline filters for contamination mitigation.

Operationally, the Kinney pump was used after the venturi pump. (For this test series, the venturi was the primary roughing pump). The Kinney pump was typically activated at about 100 Torr and was operated until the maximum pressure for the high-vacuum pumps (turbo and/or cryo) was achieved. For the phase 1 test series the turbo pump was not used, so an additional rotary vane roughing pump was used in tandem with the Kinney pump. The additional pumping capability was needed to achieve the cryo pump operating pressure. This “Welch” brand pump was plumbed directly to the chamber. The only contamination protection was the pump’s standard LN₂ cold trap. While intended to prevent oil back-streaming, it also filtered condensable gases such as water. When the turbo pump became operational during the phase 2 test series, the Kinney pump was only needed to fill the gap between the venturi pump and turbo pump (30 to 0.75 Torr).

A benefit of the Kinney pump was the ability to control the pressure decay rate (dP/dt) by opening the built-in purge lines, effectively adding a small atmospheric pressure load to the pump downstream of the chamber. The most troublesome pressure range for off-gassing soil disruptions was 1 to 10 Torr. With this control over pressure decay, pumping could be optimized while avoiding visible simulant disturbances.

2.1.4 Turbo Molecular (Turbo) Pump

Turbo pumps (Fig. 7) consist of a series of rotor blades that spin at high speed (25,000 rpm), operating similar to a jet turbine. Gases are compressed as they pass through each rotor stage, or at low pressures individual gas molecules are batted out of the chamber. Gas molecular weight does not affect pumping rate as it does for all other types of pumps. A backing pump is required to vent the exhaust gases. For this facility, a scroll pump was used. The operational range of the VF13 turbo pump was 0.75 to 10⁻⁶ Torr.

Turbo pumps can be intolerant of dust contamination and vibration or impulses. Because of the former, this pump was originally disregarded for soil mechanics tests. However, phase 1 test results indicated that soil disruptions ceased below 1 Torr, so the risk of airborne particulates in the turbo pump operating range was low. The turbo pump became the primary workhorse for phase 2 of the test program. However, a baffle plate was added to the pump inlet as a precaution to deflect airborne particulates from pump intake. Additionally, the pump was isolated from the chamber anytime the soil was robotically manipulated.



Figure 7.—The turbo molecular pump on VF13.

The pressure decay rate of the turbo pump is optimum in the 10^{-2} to 10^{-3} Torr range. When first activated at 0.75 Torr, pressure decay rate follows a power law curve fit, increasing effectiveness as pressure declines. In this range, the pump required additional cooling when under loading from the soil to prevent automatic shutdown when the casing temperature reaches 75 °C. Cooling was accomplished using a set of fans pointed at the body of the pump. A sealed bag of ice was also placed on the pump body for the first few hours of operation. The ice was no longer necessary below 5×10^{-3} Torr.

2.1.5 Cryogenic (Cryo) Pump

A cryo pump (Fig. 8) consists of a cold surface that is maintained at 20 K using helium compression. Gas molecules are condensed onto, and retained by, the cold surface. Since no moving parts are exposed to the chamber, it is a rugged pump tolerant of soil particulates. The operational range in this facility is 0.1 to 10^{-7} Torr.

The disadvantage is that the molecules themselves are not fully removed from the chamber, but remain trapped on the exposed cold surface. Eventually the cold surface saturates causing it to warm, and the pump ceases to be effective. Automatically shut-off occurs when it reaches 50 K. However, the decline in pressure decay rate typically became significant at 30 K (which is the nitrogen vapor pressure at 10^{-5} Torr), and the pump is manually deactivated by the operator. The indicators of cold surface saturation are: a temperature increase, decline in pump performance (reduced pressure decay rate), and poor thermal isolation with the outside body of the pump (condensation is a good indicator on humid days).

The procedure for cleaning off the cold surface is called regeneration (“regen”). To do this, the pump was isolated from the chamber using the large gate valve, deactivated, and allowed to return to room temperature. This typically took 3 to 4 hr. Heaters were added to the pump body to expedite warm up. The pump was then repeatedly flushed with nitrogen gas and purged with the roughing pump until the pressure in the cryo pump body reached 0.5 Torr. The purge cycle took 1 to 2 hr. The cryo pump was then re-activated, and took another 4 hr to reach the 20 K operating temperature. In total, it took between 8 to 10 hr to recover from cryo pump saturation. In larger scale vacuum facilities, multiple cryo pumps are used so that one is active while the other is regenerating. In VF13, the turbo pump was left on during these regens to minimize pressure rise in the chamber.



Figure 8.—The cryogenic pump on VF13.

The cryogenic pump was always that last pump to be activated in the test sequence. During phase 2 of the program, it was operated in tandem with the turbo pump. Tandem operation increased the pressure decay rate and, since the turbo pump actively removed gases from the chamber, delayed saturation of the cryo pump. The turbo pump could also continue to remove helium. Since helium is the working gas of the cryo pump it cannot condense it out of the chamber.

The pressure decay rates indicate a fast pressure drop when the cryo pump was opened. However, this quickly leveled out. Note that the pressure decay rates in Figure 3 are for tandem operation of the cryo and turbo pumps.

2.2 Pressure Sensors

The primary pressure sensor for the facility was a Granville Phillips multi-mode pressure gauge. The unit contains three sensor types optimized for different pressure regimes. From ambient conditions to around 10 Torr, piezo-resistive diaphragm sensors are used. The unit then automatically switches to the “conductron” sensor, which measures resistance changes across a heated wire. At around 10^{-3} Torr, the micro-ion gauge becomes active, which uses a high temperature filament to ionize gas molecules. All of these sensors were in calibration during the test program. Once the program ended, this calibration was re-verified by the manufacturer.

However, a discrepancy was noted during test 5. During the final days of test 5, there was an odd fluctuation in the pressure data, which called into question the functionality of the micro-ion gauge. The filament was degaussed, but no change was observed. To check the accuracy, a second ion gauge was added to the facility. This glass tube ion gauge replaced an identical gauge that had failed prior to the test program. The replacement was not calibrated prior to installation due to time considerations. Additionally an RGA was active and measured the partial pressures of all species with mass numbers 1 to 50. Summing these pressures yielded an approximate total pressure. The results of the three gauges are plotted in Figure 9. Note that neither the RGA nor glass tube ion gauge could be active above 10^{-3} Torr due to the filament sensitivity. The plot indicates good agreement between the RGA and the glass tube gauge, but the calibrated gauge reads higher. The error bars indicate the stated accuracy of the instruments

(15 percent for the micro-ion gauge, and 20 percent for the glass tube ion gauge). The offset between the sensors seems to scale with pressure, as shown in Figure 10. The offset is consistently 76 percent of the micro ion gauge reading. Despite the striking similarity between the RGA and the glass tube gauge, the micro ion gauge was the only sensor with a traceable calibration. Hence, it was the reportable measurement.

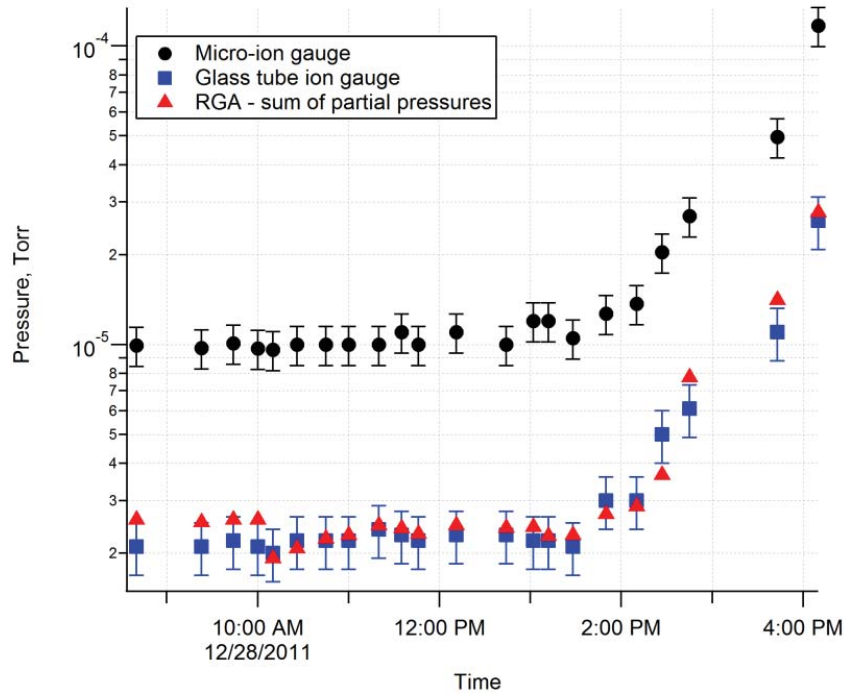


Figure 9.—Comparison of the pressure gauge measurements.

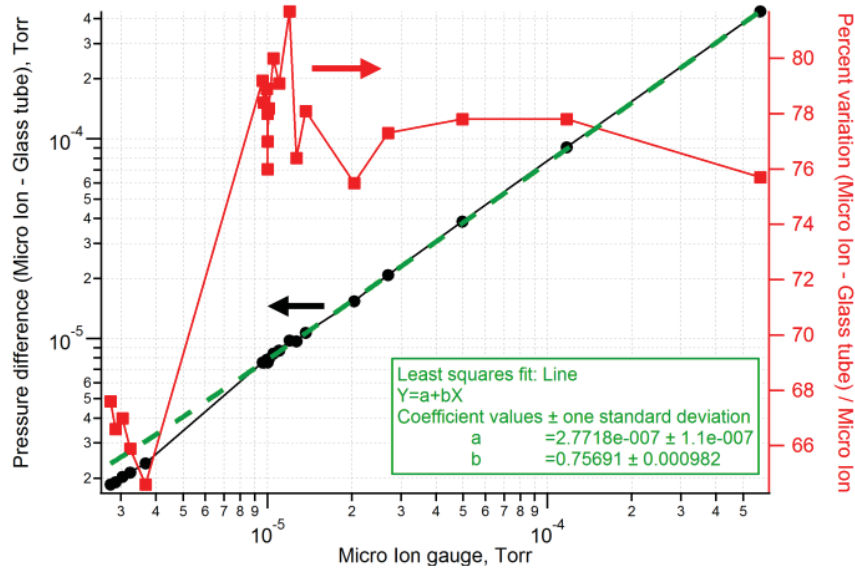


Figure 10.—The discrepancy between the pressure sensors is inversely related to pressure.

3.0 Research Hardware

Hardware build-up and operational improvements occurred in parallel with testing. Thus, different hardware was utilized as testing progressed (Table 2). All tests utilized the same soil bin, a 1 m² by 0.7 m deep box that contained roughly 900 kg of lunar regolith simulant. The soil depth was approximately 0.6 m, which is an appropriate depth for traction and surface excavation tests. The first set of tests used GRC-3 geotechnical lunar simulant while the latter tests used NU-LHT-3M. The total bin weight with soil was about 1 metric ton.

The primary diagnostic was an electric cone penetrometer (CP) which was pushed into the simulant at 0.5 cm/sec. The CP had a 2.54 cm diameter shaft with a 7.6 cm long friction sleeve and a 60° full angle cone tip. The pressure felt by the tip and the sleeve friction during penetration was recorded at 2 to 5 mm depth intervals. Qualitatively, the CP provided soil shear and compression strength as a function of depth. This is a good indicator of stratification from filling, tilling, and compaction operations. Quantitatively fitting the tip resistance versus depth data with classical soil mechanics models (Refs. 19 and 20) allows, in principle, the extraction of soil parameters like bulk density, cohesion and friction angle; maximum shear modulus, and wall friction angle for each strata. Even with $R^2 \geq 0.99$ fits observed here, the parameter values found were not unique because the heuristically developed parameters are not physically independent; causing any fit program to be confused by the coupled partial derivatives used to search for minimum residuals.

Black and white surveillance video cameras were mounted within the chamber to monitor activity within the vacuum chamber. These cameras were used by the operator to guide auger and tamper maneuvers via remote control during phase 2 and to monitor soil activity. The cameras were modified in-house by research video staff with additional heat sinks to ensure operation at low pressure, where heat rejection is difficult. Two cameras were located at opposite corners of the simulant bin, only a few inches above the simulant surface for a grazing view. Two others were mounted on the CP frame to give a top view of the bin surface and the 2D trolley equipment locations. The chamber was illuminated by diffuse green LED lights (the light color chosen solely on availability). LEDs are vacuum tolerant since they do not emit much heat. Pressure data was logged at 1 Hz over the entire test duration using the multi-mode pressure gauge noted earlier. An MKS Instruments e-Vision residual gas analyzer (RGA) was mounted on the lid of the chamber with the sensor recessed behind a valve to prevent exposure to high pressures and dust. The RGA could not be activated until the pressure reached 5×10^{-4} Torr.

In phase 2, the research hardware included a tamper and auger, in addition to the CP. All of these were housed on a 2D translation frame to move them over the soil bin. All equipment (CP, tamper, auger, and translation frame) were remotely controlled using a mixture of inductive, stepper and servo motors. The CP drive motor was a high torque feedback-controlled servo motor that was programmed with a trapezoidal shaped speed-time profile. This motor, and its gearbox and jack-screw drive train, were well suited for anticipated pushing forces and speeds. While the same motor would have been best for the auger drive, an electrical feed through limitation and long lead time on the servo necessitated the use of a stepper motor instead. This stepper motor had a limited duty cycle because of heating issues. The tamper motor was a 0 to 3600 rpm sealed inductive motor that replicated performance of a commercial

TABLE 2.—SUMMARY OF TEST CONDITIONS

	Test	Capabilities	Changes to set up and operation
Phase 1	1	Fixed frame CP; 2 cameras	Used GRC-3 and a mechanical flex shaft feed-through for the CP
	2	Fixed frame CP; 3 cameras	Dust protection measures for Kinney pump
	3	Fixed frame CP; 3 cameras	LHT-3M simulant, unattended operation of Kinney pump
Phase 2	4	2D translation frame for CP and Tamper; 4 cameras	Turbo pump operation permitted. All hardware (CP, tamper, translation) remote controlled.
	5	2D translation frame for CP, Tamper, and Auger; 4 cameras	Turbo pump cooling for continuous, unattended operation. Auger added with remote control.

construction tamper used in the large indoor soil bins at GRC. The tamper was only operated on one minute cycles, so no heating problems were evident. All positioning motors on the translation stage were stepper motors, which are easy to wire and program. Their low load and duty cycle presented no heating problems. All motors and cameras were instrumented with thermocouples to monitor temperatures at vacuum.

3.1 Phase 1 Capabilities

Figure 11 shows the phase 1 hardware. The only device used in this phase was the cone penetrometer (CP) which was held on a fixed frame bolted to the facility mounting flange. Because of the fixed frame, only one penetration could occur in each test. This was done at vacuum conditions to obtain baseline data to compare to the phase 2 tests. The CP was driven by a standard hand drill via a flexible shaft feed-through coupled to the jack-screw push drive. All lubricated surfaces of the drive system were cleaned of stock lubricants and re-lubricated with a specialty vacuum compatible lubricant (Rheolube 2000), identified by the tribology research group at GRC, to prevent degradation and off-gassing in the vacuum environment.

A total of three tests were performed during phase 1. The first two utilized GRC-3 simulant while the last used LHT-3M. The primary goal of this test phase was to refine operational procedures and improve hardware design.

3.2 Phase 2 Capabilities

In phase 2, capabilities were added to allow robotic manipulation of the simulant. In the first test (test 4), a tamper was added to enable soil compaction at vacuum conditions. In the second test (test 5), the tamper was accompanied by a cork-screw auger, for tilling the soil at vacuum. Both of these devices, along with the CP, were mounted on a mobile frame so that the entire soil surface could be accessed. Figure 12 shows the set up. All of the devices (tamper, auger, CP) are mounted on the tall center boom and can be translated across the bed surfaces using chain drives mounted to the square frame. The tamper can be seen resting on the soil surface just beneath this frame.



Figure 11.—The cone penetrometer on a fixed frame in phase 1.



Figure 12.—The phase 2 hardware assembly.

3.2.1 2-D Translation

Figure 13 shows a close up of the 2D translation frame. Motion was accomplished using chain drives and stepper motors with electrical limit switches. The chains on the outside of the frame drive the “Y” direction motion, while the chains in the center of the image drive the “X” motion. Translation was automated to a set of eleven pre-programmed positions shown in Figure 14, but manual movement was also possible. Positions 1 to 6 were chosen based on the footprint of the tamper (see section 3.2.3) to ensure compaction of the entire bed with acceptable overlaps. The color rectangles in Figure 14 indicate the tamper footprint at each position. The remaining five positions (7 to 11) were equidistant cone penetration locations. These positions are shown as numbered, red dots. Positions labeled ‘a’ and ‘b’ were manual penetration locations where the number represents the start location of manual navigation. The navigation was done at vacuum conditions using the video feed, thus the locations shown are approximate. Wire routing was carefully laid out to ensure that numerous degrees of freedom were available. Note that each square of the grid in Figure 14 is 1 by 1 in.

3.2.2 Cone Penetrometer

In phase 1 of the project, the cone penetrometer was driven using a flexible shaft and mechanical feed-through. In phase 2 it was driven by a servo motor which was translated with the cone penetrometer (Fig. 15). Like the jack-screw in phase 1 (which was re-used here), the off-the-shelf servo motor had to be opened and re-lubricated with vacuum compatible grease. A right-angle open gear was chosen to provide a 0.5 cm/s penetration rate.

The cone penetrometer was an ARA-Vertek 'mini-electric' cone with 2.54 cm diameter and 60° full angle cone. There were strain gauges and amplifiers right in the tip and sleeve to optimize signal to noise. The cone dynamic range was 0 to 9 kN (0 to 17.76 MPa) with 0.2 percent accuracy. A string potentiometer provided depth readings for each tip resistance value. The data acquisition electronics and software were stock items associated with the cone penetrometer.

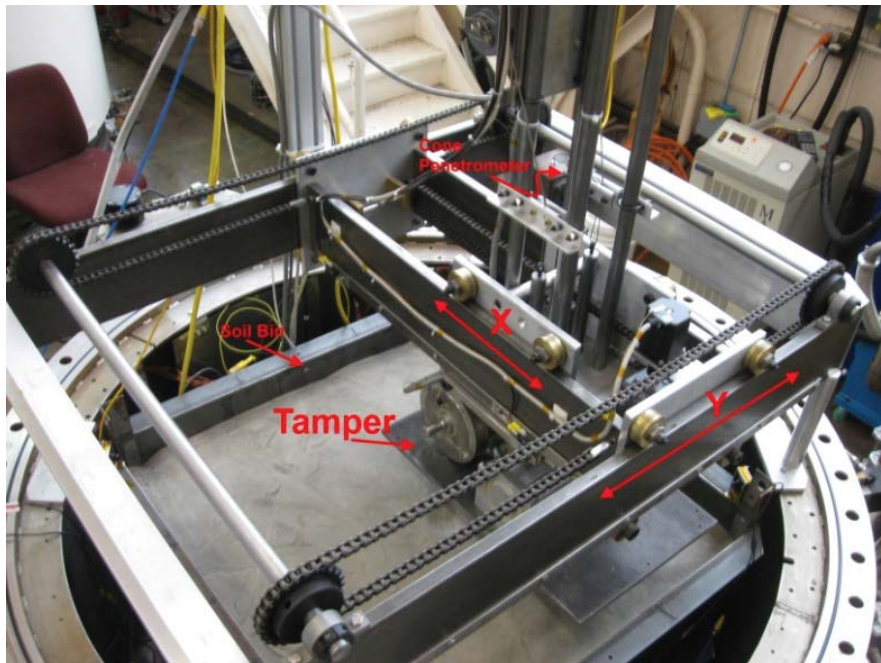


Figure 13.—The 2D translation stage for positioning the auger, tamper, and CP.

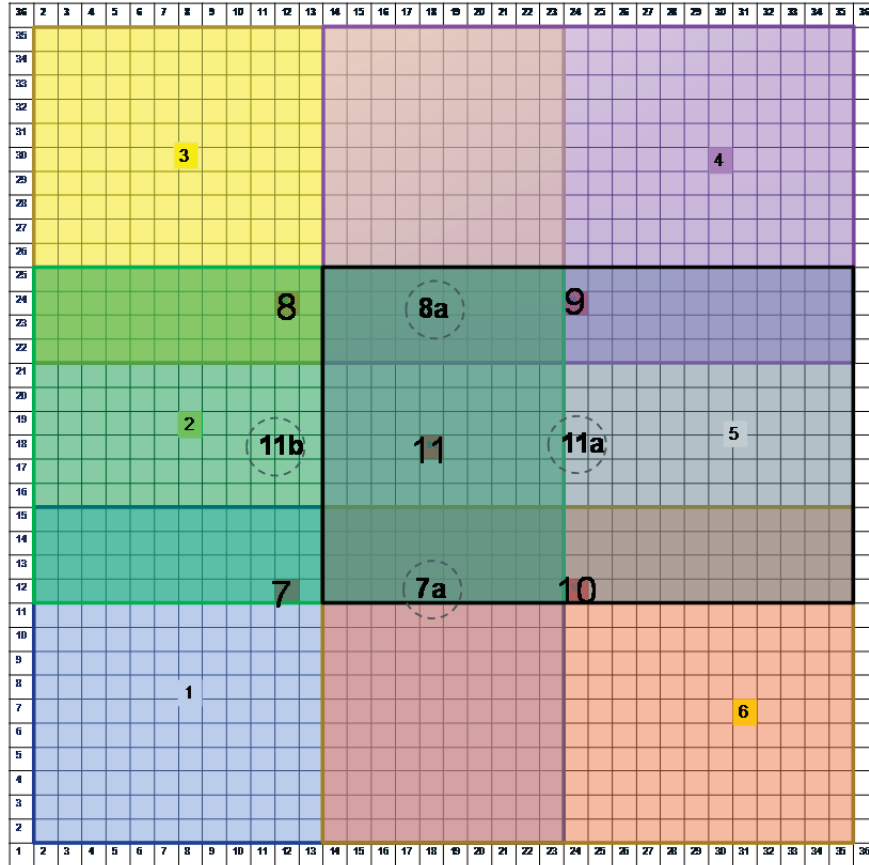


Figure 14.—Pre-programmed positions for the translation stage. The foot print of the tamper is shown at each tamp position (1 to 6), while positions 7 to 11 show the penetration points. Each square of the grid is 1 by 1 in.

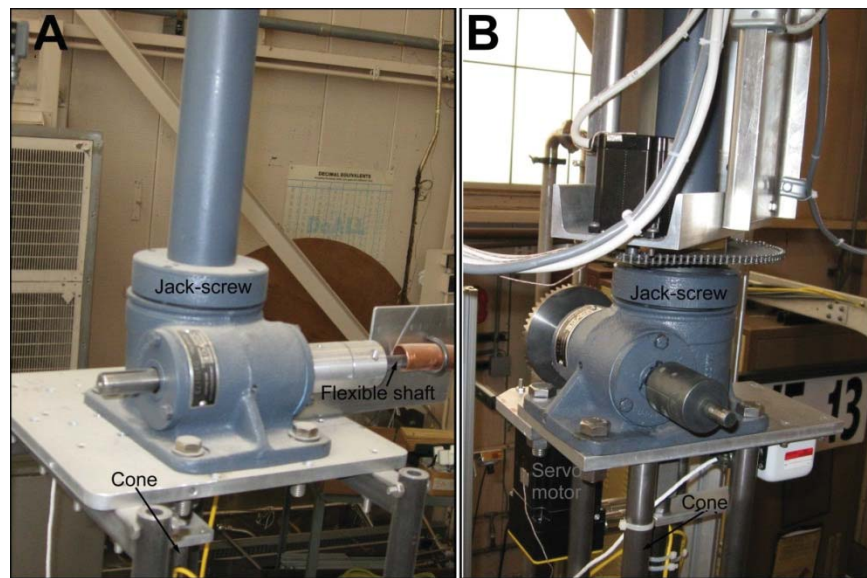


Figure 15.—The drive system for the cone penetrometer during phase 1 (A) and phase 2 (B).

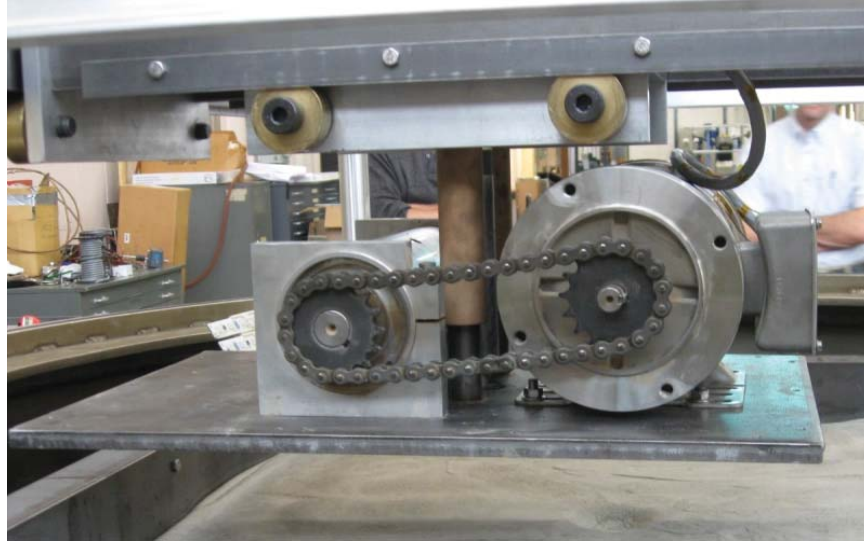


Figure 16.—The tamper used for soil compaction at vacuum conditions.

3.2.3 Tamper

The tamper, shown in Figure 16, consists of the 3 phase, 0 to 3600 rpm induction motor (right) which rotated an eccentric cylindrical weight. The speed of the motor could be varied to adjust the tamping power, which was applied to the soil via the 14 by 22 in. base plate. The vibration resulted in up to 55 kPa at the surface at up to 5000 vibrations/second, comparable to walk-behind tampers at construction sites. A stepper motor was also installed to raise and lower the tamper in 0.5 in. increments via a pair of cables and pulleys. When tamping, these cables had to be lowered with sufficient slack to ensure the full weight of the tamper was born by the simulant bed and did not stress the frame. The controlled increments enabled repeatable lowering and cable slack for consistent tamping.

The tamper was only operated at vacuum conditions. The soil bin was compacted by moving sequentially through positions 1 to 6 on Figure 14. Various tamper speeds were attempted during the test 4, including slow ramp up. At some speeds structural resonances of the vacuum chamber and building floor were encountered, so these settings were avoided. Standard operation for test 5 was a 50 percent motor speed, with no ramp up, sustained for 15 to 30 s at each location. Running the tamper for longer times or higher speeds resulted in heaving up of previously tamped areas. The entire bed was tamped two times, with some locations tamped three times in test 5. Tamping in vacuum was much less dusty than in ambient because of the lack of interstitial and surface air blowing material around.

3.2.4 Cork-Screw Auger

The auger was added for test 5 to till the soil. This provided a means of resetting the soil state at a vacuum to better gauge the vacuum compaction effectiveness. This capability also made it possible to run several tests (compaction, penetration) in a single pump down cycle. The auger was also used at various points during pump down to encourage off-gassing from the soil. Figure 17 shows the auger in the process of tilling the bin prior to pump down.

Three stepper motors were used to control the auger. One was used for auger rotation (spin) and another for z-direction (up/down) motion. The auger was also mounted to a 270° swing arm controlled by the third stepper motor. This, in conjunction with the 2D translation, allowed access to the entire bin surface. When actively tilling the soil the auger would spin continuously, while driven into the soil at the operator's discretion. Leaving the auger to spin in place while partially buried was effective for encouraging off-gassing, as it brought deeper materials to the surface. A perceptible swelling of the soil volume was apparent in the box after tilling.

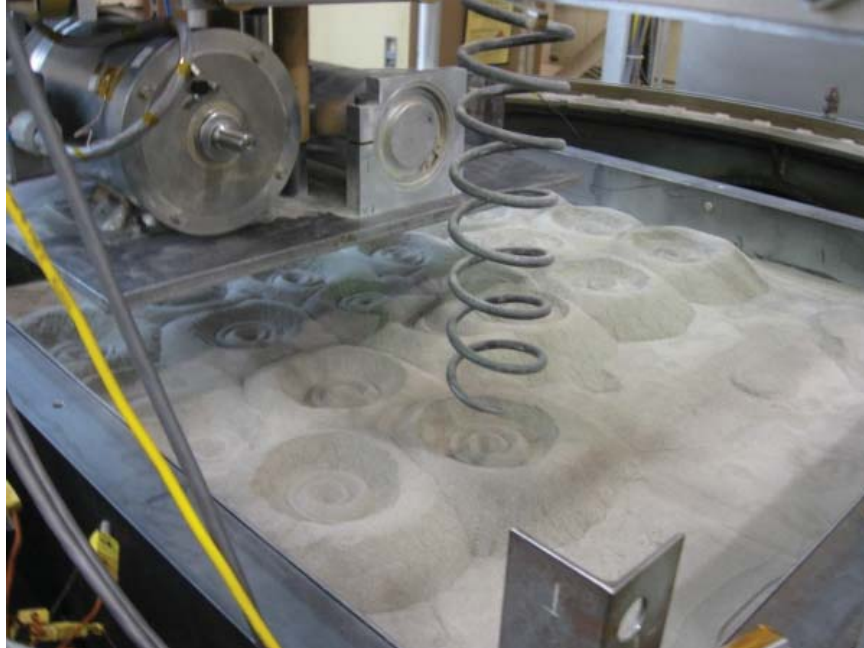


Figure 17.—The auger is shown tilling the soil at room conditions.

4.0 Results and Discussion

The following sections detail the behaviors of both the facility (the pressure response) and the soil (gas release, compaction, and CP test).

4.1 Pressure Environment

The target pressure for soil operations was 10^{-6} Torr or less. The baseline data indicates that the facility itself is capable of achieving this target. However, any object in the chamber that has been exposed to atmospheric pressure and/or handling (including the chamber surfaces themselves) will off-gas at reduced pressure. The presence of the soil alone represented a considerable gas load from the interstitial gases and high surface area of adsorbed water, both of which slow the pump down process. The time it would take to completely off-gas a 1 ton soil bin was prohibitive under our time and resource constraints. Thus, the goal was to reach a pressure in the target range with the pumps running. This alone took a week to achieve. Once the pumps were deactivated, the pressure would rise to an equilibrium vapor pressure. Thus soil operations were performed with the pumps running when possible. This is not ideal in terms of soil conditions (since volatiles are still present and actively releasing from the soil) but is adequate to examine hardware behavior and most mechanics of soil interaction.

Heating the soil bin was considered to drive off volatiles more expediently. But this may result in an unknown soil inhomogeneity from heat propagation and drying from the boundaries. Ultimately this capability should be added and time allowed for full off-gassing to see if it makes a measurable geotechnical difference. The vacuum regolith/simulant literature (Refs. 2 to 12) makes clear the effects complete off-gassing has demonstrated for small soil samples. Some papers suggest that ASTM soil mechanics drying practice at 105 °C is not sufficient to establish the anhydrous particle conditions common on the moon. On the order of 600 °C is recommended. That was beyond the resources of this effort.

The pressure logs from the tests provide insight into soil off-gassing as well as facility logistics. Figure 18 shows the pressure logs from all five tests. Note that all tests lasted a week or more. Hardware and procedural improvements in each test resulted in lower pressures achieved in shorter times. Refer to Table 2 for a summary of test conditions.

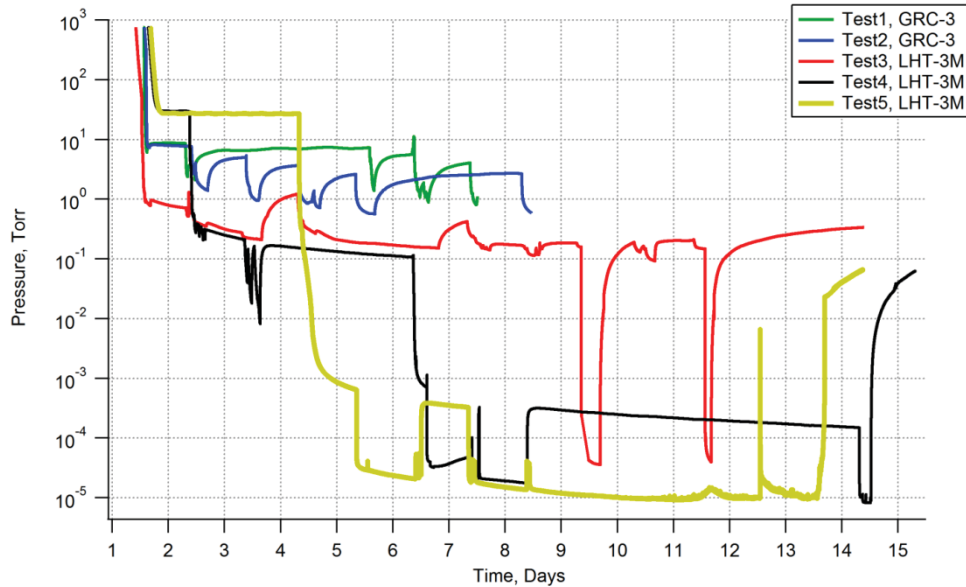


Figure 18.—Pressure logs for all five vacuum tests.

Test 1: The initial (day 1) pump down was done with the Kinney roughing pump and the secondary “Welch” roughing pump. This resulted in a high pressure decay rate which lead to a variety of soil disruptions that will be described in a later section. The pumps could not be operated unattended, so were shut down during nights and weekend. When the pumps were isolated and deactivated, the pressure rose to its equilibrium value. The long pressure hold through days 3 and 4 represents a weekend, while the sawtooth shapes at the end of days 5 and 6 are overnights. Note that the pressure was stable during the weekend, indicating a good chamber seal. The lowest pressure was achieved on the last day was 0.8 Torr, which was not low enough for cryogenic pump activation. However, the cryo pump was forced open at about 4 Torr in an attempt to expedite the pump down (with the expectation that an immediate regeneration would be needed). This resulted in a rapid depressurization and a large soil disruption. The pump immediately saturated and was deactivated. The pressure quickly rose back up to 4 Torr, so the scenario did not prove beneficial. The test ended when the Kinney pump seized. This was initially thought to be caused by dust contamination, but later was shown to be a pre-existing flaw in the pump. Nevertheless, extra precautions, described in section 2.1.3, were taken to protect the replacement pump from dust in subsequent tests.

Test 2: The venturi pump was activated at atmospheric pressure, followed by the two roughing pumps at 300 Torr. The lower pressure decay rate of the venturi seemed to prevent soil disruption in this higher pressure range. The saw tooth shapes again represent the overnight periods when the pumps had to be shut down. The lowest pressure achieved was 0.5 Torr, thus the cryo pump could not be activated. The test was ended in the interest of time, so that facility improvements could be initiated. This primarily included the addition of software to enable unattended operation of the pumps.

Test 3: Like the previous test, this test began with the venturi pump and was followed by the roughing pumps at about 50 Torr. Only two highly localized soil disturbances were observed when the roughing pumps were activated. The control system was modified so that the Kinney pump could operate unattended. This prevented the overnight pressure rises seen in tests 1 and 2 and expedited the process. The pump did shutdown during the evenings of days 3 and 6 when the failsafe condition was triggered (likely a power flicker due to thunderstorms). The Kinney pump performance deteriorated significantly at 1 Torr, resulting in a slow pressure decline after day 3. However, by day 9 the pressure was low enough to activate the cryo pump, resulting in the sharp pressure decay. The cryo pump saturated by the end of day 9 and had to be regenerated. It was reactivated during day 11, resulting in the second sharp pressure decline. The lowest pressure, achieved with the cryo pump, was 4.3×10^{-5} Torr.

Test 4: This was the first test of phase 2, and thus took place three months after the previous test. During this time the turbo pump was readied for use. Results from tests 1 to 3 indicated that the risk of soil contamination at the turbo pump's operating pressure (0.75 Torr) was minimal. The use of the turbo pump accounts for much of the gain made in this test. Again, the venturi pump was activated first. This time it was activated in the afternoon and allowed to pump overnight, reaching a pressure of 30 Torr. It reached this pressure in 4.5 hr and held stable until the Kinney pump was activated. The Kinney pump was only needed for ~1 hr, and then the turbo pump was activated. However, the heavy gas load resulted in overheating of the turbo pump, and it had to be shut off intermittently to cool. This explains the pressure spikes seen in day 2 and 3. On day 6, after a weekend, the turbo pump could remain on without temperature issue. The cryo pump was also activated on day 6. The cryo pump required regeneration by day 8 and was deactivated to do so. However, difficulties in the regeneration (leak in the purge valve) and a long holiday weekend prevented cryo pump reactivation until day 14. The lowest pressure was 8×10^{-6} Torr on day 14.

Test 5: As with the last test, the venturi pump was activated in the late afternoon of day 1. The pressure again reached 30 Torr within about 4.5 hr and held steady at that level over a weekend (days 2 and 3). The roughing pumps were only on for 1 hr on day 4 before the turbo pump was activated (the roughing pumps were shut off about 20 min after the turbo pump was activated). To prevent over-temperature, the turbo pump was cooled with fans and sealed ice bags. This prevented the intermittent shut down that hindered test 4. The ice cooling was removed after 6 hr when the pressure reached the 10^{-3} Torr scale. On day 5 the cryo pump was activated, resulting in a pressure drop to 6×10^{-4} Torr. The cryo and turbo pumps were run in tandem. Other than a cryo regeneration on day 6 and 7, both pumps continued operation until day 13. The pressure spike at day 12 was caused by the replacement of a failed glass tube ion gauge (the internal volume of the sensor caused the spike). The lowest pressure reached was 9×10^{-6} Torr.

4.1.1 Pressure Comparison to Baseline

Figure 19 illustrates the effect the hardware and soil had on the pump performance. The data from test 5 (red) is plotted with the baseline pressure test (black). The pump(s) active during each time segment are listed at the top. The time scales are such that time of zero corresponds to the activation of each pump. The time scales are linear in Figure 19(A) to emphasize the strong variation in pump down times (especially in the case of the turbo and cryo+turbo pumps) and logarithmic time scale in Figure 19(b) to emphasize the trend similarities during the pump initiation. The pressure decay of the venturi was the same with and without the soil bin. For the baseline test, the Kinney pump performance had just begun to asymptote after 1 hr, reaching 0.1 Torr. However, in test 5 the pressure decay rate began to asymptote after only 30 min to a pressure of 0.4 Torr. Soil gas release is the expected cause of decreased Kinney performance. The soil load affected the turbo pump similarly. In both cases the turbo pump performance begins increasing at 10^{-1} Torr and then after an inflection point in Figure 19(B) decays to a constant slope until the cryo-pump is activated. It took 6 hr to reach a pressure of 2×10^{-3} Torr in test 5, while this only took 10 min in the baseline test. Similarly, when the cryo pump was activated there was a sharp pressure decline in both tests, leveling out to constant linear slope in Figure 19(a). While the time scale of the sharp decline was similar, the pressure in test 5 leveled out at 5×10^{-5} Torr and in the baseline test an order of magnitude lower.

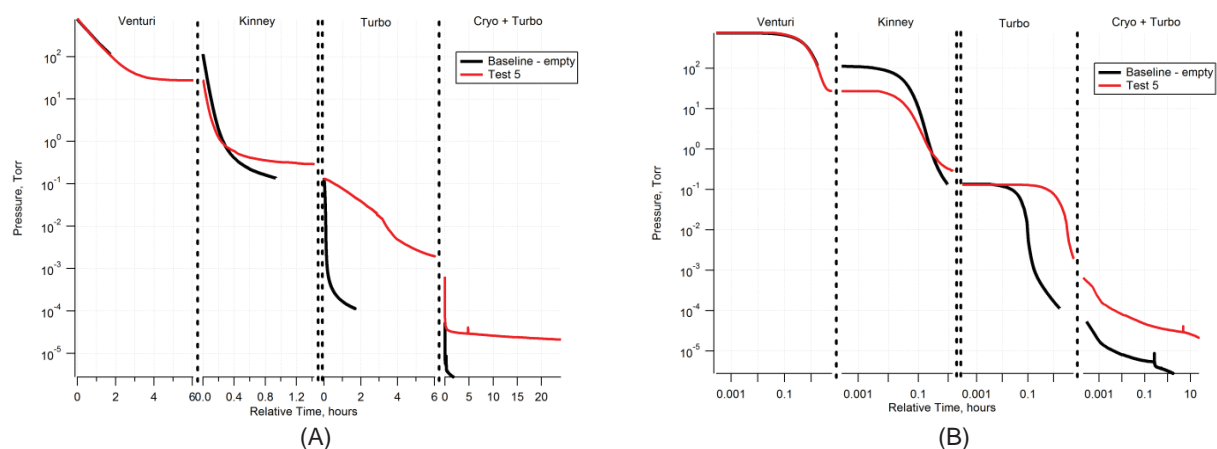


Figure 19.—Comparison of pump performance with (test 5) and without (baseline) soil and compaction hardware.

4.2 Soil Disruptions

Simulant disruptions can occur when gases, trapped within the simulant bed, release in a low pressure environment. This includes gases trapped within the particle pore structure, as well volatile species (such as water) adsorbed to the particle surfaces. Several types of simulant disturbances were observed, with examples shown in Figure 20. Figure 20(A) was taken during test 2 and shows two disturbance types. The localized disturbance shown in the foreground is characterized by small, isolated craters that issue forth small amount of loose simulant. The appearance of these disturbances is very similar in appearance to boiling (though the phenomena is itself is unrelated to boiling, e.g., liquid-gas phase change). These are small scale disturbances with little perceivable elevated dust generation. In contrast to this is the 'wave-like' eruption in the image back ground. A wave eruption starts as a simulant spout (geyser) and quickly grows and propagates like a wave over the surface. A significant amount of elevated dust is generated. A 'crawling wave' (not shown) is similar to this but on a smaller scale and without noticeable dust generation. In these disturbances it appears as though a creature is moving just beneath the surface. A surface disturbance is shown in Figure 20(B). This event from test 1 shows small scale disturbances over the entire surface. This disturbance was also similar in appearance to liquid boiling, but unlike the localized “boil” described above, these disturbances unpredictably moved over the entire surface. Figure 20(C), from test 3, shows a post-test image of a simulant spout. Spouts were observed in tests 1 to 3 and were always isolated to the corners of the bin. They remained fixed in location and could persist for several minutes. This was the only simulant disturbance that occurred with the LHT-3M simulant (in test 3 only) while all other disturbances occurred with GRC-3 simulant in tests 1 and 2. Comparing test 2 with GRC-3 and test 3 with LHT-3M under similar early pump down profiles, LHT-3M showed less propensity to soil disruptions. Bin filling with GRC-3 was a single one ton soil dump, whereas many 20 to 30 kg buckets of LHT-3M were gently poured, so there may be consequences in how the interstitial gasses were trapped. However, GRC-3 had undergone interstitial gas removal during test 1 followed by a month of time consolidation in ambient conditions before test 2. This should alleviate the effects of different filling history by the time of test 2. The cone penetration traces show GRC-3 was stronger in test 2 than in test 1 throughout the penetration depth, consistent with a more dense state in test 2. The same LHT-3M simulant used in test 3 had no activity during tests 4 and 5, further suggesting LHT-3M may be less prone to soil disruptions.

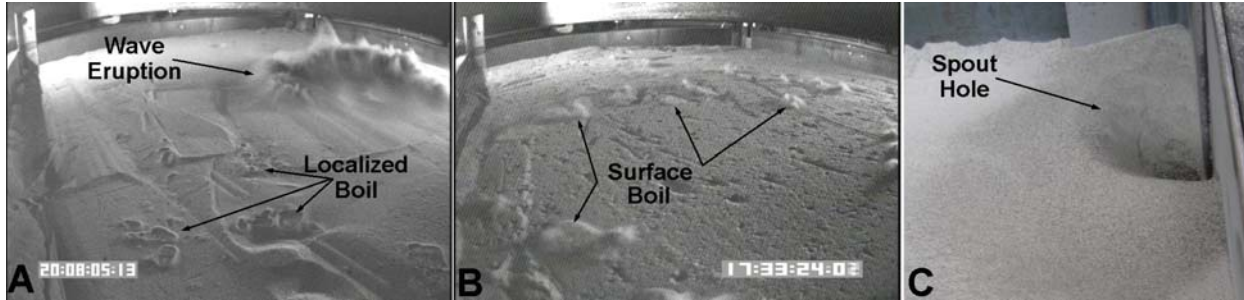


Figure 20.—Photos from the video showing the different types of simulant disturbances. Note that 'boil' describes only the appearance of soil disturbance, and is not related to an actual liquid phase change.

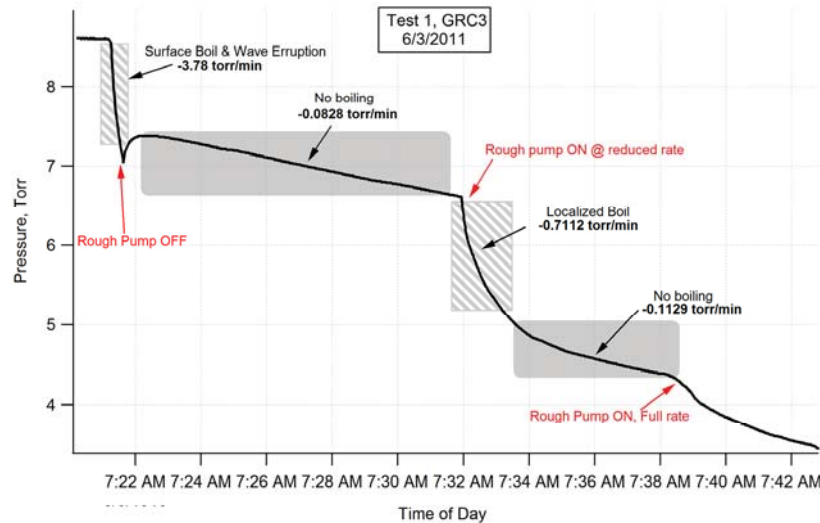


Figure 21.—The pressure log from a portion of test 1. The periods where simulant disturbances were observed are shown, along with pressure decay (pump down) rates based on linear curve fits of the data.

Simulant disturbances were most prevalent when the pressure differential across the simulant bed was high; in other words, when the pressure decay rate was high. This is illustrated in Figure 21, which shows the pressure log for a portion of test 1. The two roughing pumps were initially activated concurrently, resulting in a 'fast' pressure decline and a wave eruption simulant disturbance. As soon as the disturbance was observed, the Kinney pump was closed off, leaving the smaller Welch pump acting alone. The pressure decay rate slowed considerably, and the simulant calmed. The Kinney pump was then reactivated using a nitrogen bleed to reduce its pressure decay rate on the chamber. This resulted in a lesser simulant disturbance (localized boiling). As dP/dt naturally decayed, the simulant calmed. The simulant disturbance events for each test in phase 1, along with the representative pressure decay rates are shown in Table 3 and graphically in Figure 22.

Note that there were no disturbances in tests 4 and 5, in part since the tests 1 to 3 data was used to regulate dP/dt to avoid them. This simple dP/dt analysis of the data is not adequate to determine if a rate versus pressure threshold exists for simulant disturbances. It is plausible to expect that simulant material and its consolidation distribution in the volume would affect the number and nature of the disturbances. Nevertheless, regulating the pressure decay rate does mitigate simulant disturbance.

Simulant disturbances were not observed under 2.5 Torr in any test. This includes cryogenic pump activation in test 3 which reduced the pressure from 0.15 to 5×10^{-4} Torr within 30 s. Most activity occurred in the 2.5 to 10 Torr range. This is a regime where the mean free path of gas molecules is similar to or somewhat larger than the size of interstitial voids in the simulant.

TABLE 3.—SIMULANT DISRUPTION EVENTS FOR EACH TEST WITH THE CORRESPONDING PUMP RATE AND PRESSURE RANGE OF THE EVENT.

	Event	Slope, Torr/min	Pressure range, Torr
Test 1	Spout	307	754 to 378
	Surface 'boil' → Wave eruption	-3.8	8.53 to 7.26
	Localized 'boil'	-0.7	6.55 to 5.19
Test 2	Localized spout	-53	293 to 64.5
	Localized 'boil'	-3.6	25.5 to 15.2
	Wave eruption	-1.4	7.32 to 6.33
	Crawling waves	-0.2 -0.1 -0.04	6.89 to 4.91 4.93 to 4.41 3.31 to 2.64
Test 3	Spout	-7.0	50.9 to 15.6
	Spout	-0.7	13.4 to 7.66

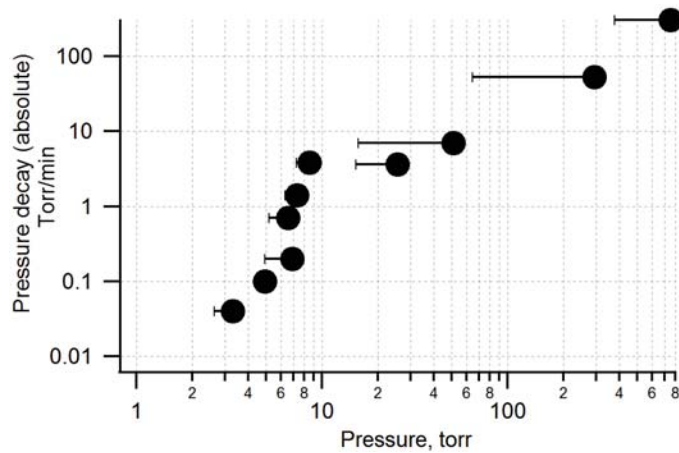


Figure 22.—Approximate pressure decay rates are shown for each simulant disturbance. Rates are plotted against the pressure in which the disturbance was first observed, and error bars show the end pressure.

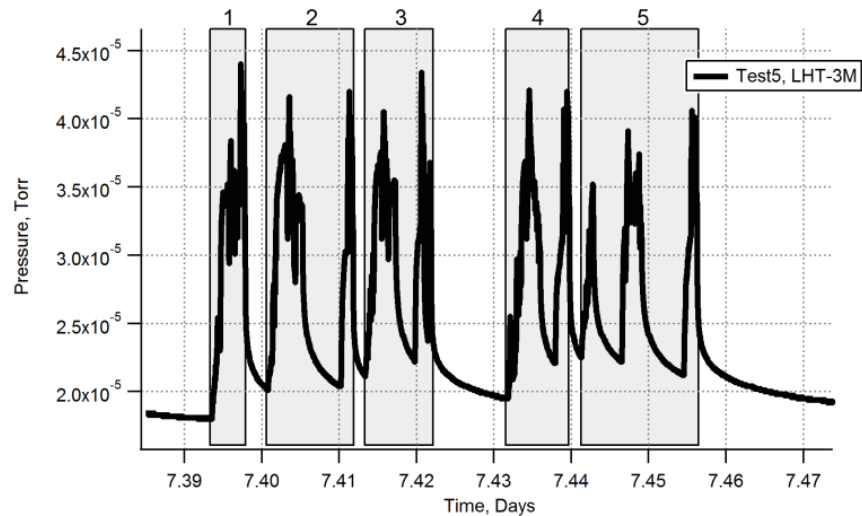


Figure 23.—Pressure response during tilling. Each highlighted regions represents a till hole.

4.3 Tilling

The cork-screw auger was only installed for test 5, and was used prior to pump down at atmospheric conditions and later under vacuum. The pre-test tilling was done to effectively ‘reset’ the consolidation state after the vacuum compactions during test 4. Figure 17 shows this tilling process. A section of the bin was left untilled so this capability could be tested at reduced pressure where it functioned equally well.

While the main goal was to reinitialize the consolidation state of the soil prior to compaction, following geotechnical standard practice, the auger also encouraged adsorbed gas release. This was evident in both the pressure and the RGA data. Figure 23 shows the pressure trace during a sequence of 5 tilling operations in different locations in the bin. All of these locations had been previously tilled. Pressure increased about 2.5×10^{-5} Torr during each operation. The spikes generally occurred while the auger was being driven either up or down in the soil. But allowing it to rotate at a fixed depth resulted in continuous off-gassing (pressure was maintained at an elevated level). On occasion, the auger had to be deactivated while at depth (rotation ceased) to allow the motor to cool. This resulted in the pressure dips seen in numbers 2 to 5 in Figure 23. The highest pressure peak was at the end of the tilling operation. The auger was allowed to rotate as it was raised, where the direction of rotation would tend to drive the auger down. This mismatch seemed to cause the most agitation to the soil, and thus a higher degree of off-gassing.

4.4 RGA

A residual gas analyzer was used to identify what gases were being off-gassed during pump down and soil operations. The RGA could only be active when the total chamber pressure was less than 5×10^{-4} Torr. Thus it was only used in tests 3, 4, and 5. Since test 5 had the most complete data set, it is shown in Figure 24. Tests 3 and 4 showed a similar distribution of gas constituents. The primary component is water and its decomposition products, such as OH. This is followed by nitrogen and carbon dioxide. These gases are also large components of air. However, if the source were air (as from a chamber leak) one would expect nitrogen to dominate. This is evidenced in day 12 where a large pressure spike occurred when a malfunctioning pressure gauge was replaced. Residual air in the gauge cavity caused the pressure rise. (Note that this pressure peak is truncated in the RGA data since the sensor was temporarily shut off for protection). The residual air caused a high nitrogen peak, which exceeded the water signal.

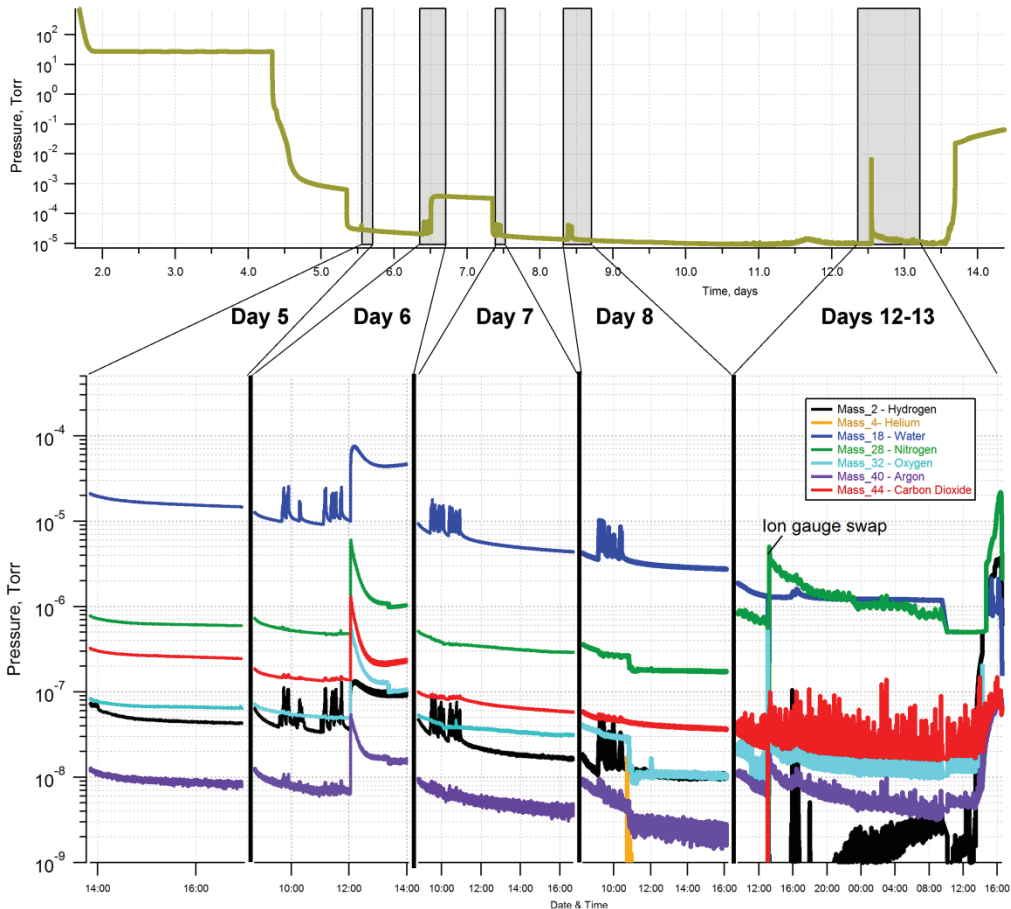


Figure 24.—RGA results from test 5.

In days 6, 7, and 8, there are a series of jagged peaks that correspond to tilling operations. Water and hydrogen were the primary gases released during tilling. These peaks did not occur when the hardware was operated with no soil interaction. In other words, the off-gassing did not come from hardware (motors), but from the soil itself. The pressure rise at the end of day 13 occurred during tamping operations. Since the tamper could not be operated without soil interaction, it was not possible to gauge how much, if any, of this off-gassing was from the tamper hardware, versus off-gassing from the soil. As with the tilling, hydrogen and water were released as the soil was disturbed. Only the cryogenic pump was run during this tamping to protect the turbo pump from particulate so some pressure fluctuations may be a result of the cryogenic pump cycling.

During days 13 and 14, there is noise on the carbon dioxide trace, and to a lesser extent on the nitrogen and water measurements. It is also evident on the facility's total pressure ion gauge, which is where the noise was first noticed during testing. Originally it was thought to be sensor error on the ion gauge. The filament was degaussed and a secondary ion gauge (the glass tube ion gauge) was added to verify the measurement (described in section 2.2). On post processing of the RGA data, these fluctuations were corroborated. The cause may be the cryogenic pump which was operating near its maximum temperature limit. If the cold surface was approaching saturation, it could be in an equilibrium state for some species. Continuous off-gassing and reabsorbing could cause minor pressure fluctuations that were noticeable at this scale.

4.5 Cone Penetrometer Test and Compaction

The cone penetrometer results for all of the LHT-3M tests are shown in Figure 25, with further detail of each penetration in Table 4. Note that single penetration from test 3 is included with the test 4 results in Figure 25. The bin was filled with LHT-3M simulant from sequential 5 gal buckets. No other soil preparation was done prior to test 3, thus the simulant stratification remained in an ‘as filled’ configuration. Only one CP measurement could be made during test 3, due to the fixed position CP frame, and this was done at vacuum conditions. The soil then remained undisturbed at ambient conditions for 2.5 months prior to test 4. The peak tip resistance showed no significant change. There is a significant stratification effect seen below 0.35 m in penetration 3-1 that is gone in penetration 4-1, either because of time consolidation or lateral inhomogeneity of consolidation in the bin, or both. After 4-1, the simulant spent 13 days under vacuum pump down. This vacuum exposure resulted in higher peak tip resistance for penetrations 4-2 and 4-3, a larger integral of the tip resistance over the full depth (energy/area), and a similar stratification as seen in 3-1. The soil bin was then compacted once in every location according to Figure 14. Penetrations 4-4 and 4-5 reflect the markedly higher peak tip stress and energy/area integral that resulted, with some variation according to bin location. After a second compaction, three more penetrations were performed, again with larger peak tip stress and energy/area integrals. Note that 4-6, the

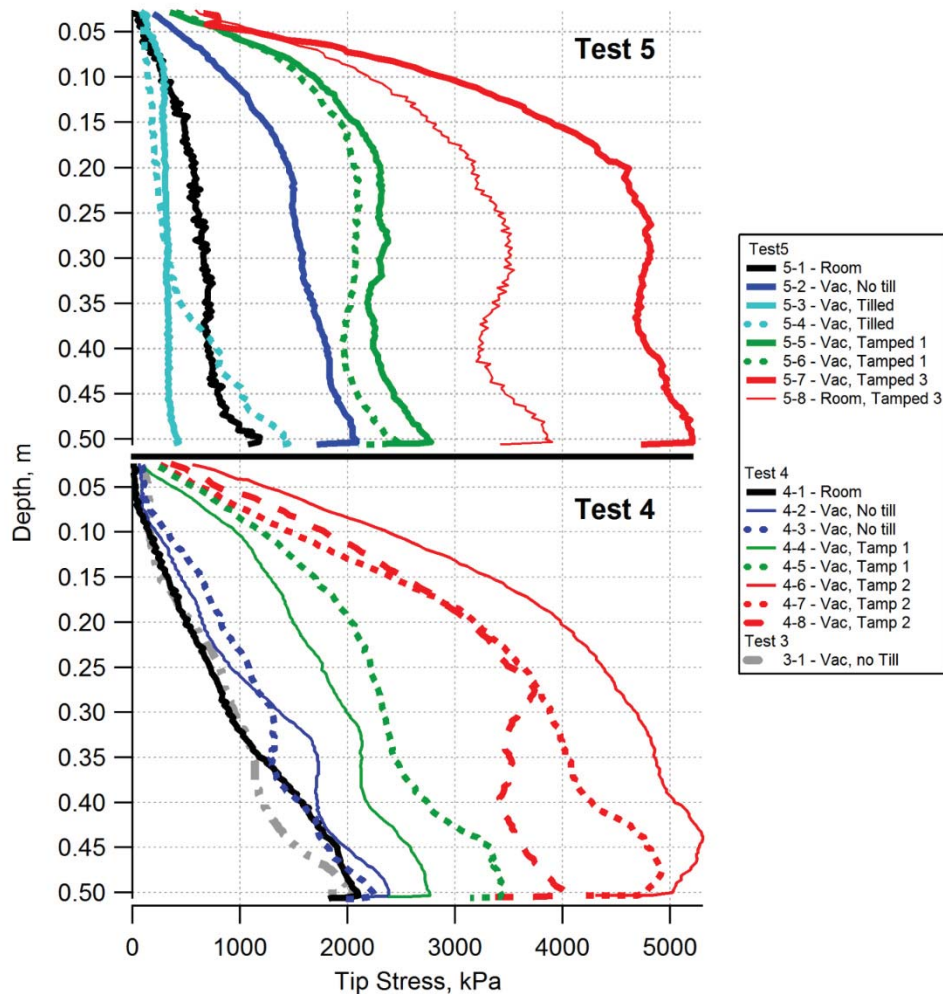


Figure 25.—LHT-3M cone penetrometer results. Where “vac” indicates a penetration at vacuum, and the number of tamps is indicated in the legend.

TABLE 4.—CP TEST DETAILS FOR LHT-3M TESTS. NOTE THAT TYPICAL ATMOSPHERIC, OR ROOM, PRESSURE IS ABOUT 755 TORR

ID	Bin Location	Pressure, Torr	Soil conditions	Active pumps
3-1	11	4e-5	As filled	
4-1	9	Room	As left by test 3	None
4-2	7	9e-6	As left by test 3	Turbo + Cryo
4-3	10	9e-6	As left by test 3	Turbo + Cryo
4-4	8	9e-3	1 compaction	None
4-5	11a	1.1e-2	1 compaction	None
4-6	9	1.4e-2	2 compactions	None
4-7	8a	1.5e-2	2 compactions	None
4-8	7a	1.6e-2	2 compactions	None
5-1	8	Room	Tilled	None
5-2	6	1.6e-5	2 compactions from test 4	Turbo + Cryo
5-3	9	1.6e-5	Tilled (pre vac + @ vac)	Turbo + Cryo
5-4	11	1.6e-5	Tilled (pre vacuum)	Turbo + Cryo
5-5	7	5.1e-2	1 compaction	None
5-6	8	5.1e-2	1 compaction	None
5-7	11a	5.5e-2	3 compactions	None
5-8	11b	Room	3 compactions	None

highest peak stress, was performed in the same location as 4-1 after two tamping operations. Penetrations 4-6 and 4-7 show some weakness near the bottom of the bin. Given the number of penetrations, this may have been influenced by nearby penetrations. Notice that 4-2 through 4-5, 4-7, and 4-8 show a qualitatively similar stratification starting around 0.3 m depth.

LHT-3M sat in ambient pressure for 17 days between the end of tests 4 and the beginning of tests 5. The bin was tilled at ambient conditions prior to penetration 5-1. If one compares 4-4 and 5-1 done in the same location, the residual stratification from the filling process is gone and the peak stress is understandably reduced from 4-4. Penetrations 5-3 and 5-4, which were tilled at vacuum, show even lower peak stress. The area at 5-3 was tilled twice and shows a fully loosened state. At 5-4, a firming below 0.35 m that suggests the auger did not go to the bottom. An exception was 5-2, which was at an un-tilled location that still had the consolidation state from test 4 (2 compactions). The peak stress is lower than comparable test 4 runs (4-6,4-7,4-8). This area was then tilled, and the bin underwent a single compaction. Penetrations 5-5 and 5-6 show similar peak stress as the comparable 4-4 and 4-5 runs, but the stratification of test 4 is no longer evident. A different stratification appears now with greater soil strength at shallower depths and not much increase at deeper depths. This is likely because surface tamping operations have less affect the farther from the impact surface. Penetration 5-7 was performed after compacting the bin three times, but shows similar peak stress as the two compaction runs in test 4. This may reflect a maximum in compaction possible for this set up. One additional penetration, 5-8, was performed after test 5 at room conditions. Its peak stress was 75 percent of the vacuum level. Figure 26 shows an image of the two penetration holes with a clear difference in the surface fracturing behavior.

One can compare vacuum versus non-vacuum soil strength from this data. Comparing as vacuum versus non-vacuum data under pairwise similar consolidation states (penetrations 4-2 versus 4-1 and 5-7 versus 5-8), the vacuum penetrations give greater peak resistance and energy/area integrals. Comparing 5-3 versus 5-1, the vacuum simulant is weaker. 5-3 was doubly tilled, with the second tilling done under vacuum, making the consolidation state not quite equivalent to 5-1. It suggests that tilling under a 10^{-5} Torr vacuum, where surface cleanliness is enhanced, leads to a weak low void ratio packing configuration. 5-3 is an interesting vertically uniform low consolidation state. It reflects the ideal initial state for controlled compaction levels to follow.



Figure 26.—Comparison of penetrometer holes from runs at vacuum (5-7) and ambient (5-8) conditions.

5.0 Conclusions

A set of tests were performed to explore pressure effects on lunar simulant. Previous, smaller scale simulant tests indicated that off-gassing of the soil during vacuum pump down caused disruptions to the preconditioned simulant state. Possible methods for mitigating this, such as pre-drying the simulant, are not feasible for the larger scale bins that would be required for ISRU hardware testing. The goal of this initial test series was to identify the conditions that cause simulant disturbances, explore options for mitigating these disturbances, and examine logistics for these larger scale tests. As such, a vacuum chamber facility at the NASA Glenn Research Center was modified to accommodate a 1 m² by 0.6 m deep simulant bed. This is the largest simulant bed tested in a vacuum to date.

Five tests were performed over the course of the test program. The first three occurred during phase 1, which was a simple set up to explore operational logistics and mitigation techniques for the soil disruptions. Only the soil bin and the cone penetrometer on a fixed frame were installed in the vacuum chamber for phase 1. In these tests, vacuum pump operation was optimized to expedite pump down. Two tests were performed in phase 2, with additional hardware to allow 2D positioning, tilling, compaction, and cone penetrometer tests at vacuum conditions. All of these components could access the entire soil surface.

Slow off-gassing of the simulant resulted in long pump down times. This can be attributed to the permeation of the volatiles through the soil depth and small pore size of the simulant particles. Since the primary volatile species was water, as indicated by the RGA data, re-absorption onto surface particles may also contribute. Continuous operation of the pumps was critical to this process, so modifications were made to permit unattended pump operation starting in test 3. The slowest portion of the pump down during phase 1 testing was in the range between 1 and 0.1 Torr, since the performance of the Kinney roughing pump falls off significantly below 1 Torr. The addition of the turbo pump in phase 2 marginalized the roughing pump and helped stave off saturation of the cryogenic pump at lower pressures. The turbo pump became a primary workhorse for phase 2.

Interstitial gas release resulted in simulant disruptions during the 760 to 1 Torr regime of phase 1. The frequency and intensity of these were affected by the pressure decay rate. Localized disruptions at slower pressure decay rates may be more manageable in a system configuration, whereas the larger disruptions at rapid pressure decay rates would alter simulant consolidation. Pumping rates were regulated in phase 2 such that no disturbances occurred. Disruptions were more prevalent in the GRC-3 simulant (tests 1 and 2), whereas LHT-3M (test 3) only had one highly localized disturbance. This may be attributed to the more porous filling history and higher water content of the GRC-3. No soil disruptions were observed below 2.5 Torr for any simulant, regardless of the pressure decay rate. It was this discovery that permitted the use of the turbo pump in phase 2, which was used in the <0.75 Torr regime to improve pressure decay rate. Since turbo pumps are sensitive to dirt contamination, they were initially disregarded. Baffling the input and operating during simulant quiescence enabled robust turbo pump use.

During phase 2, the soil was manipulated robotically using a tamper (tests 4 and 5) and an auger (test 5). Tilling operations with the auger encouraged off-gassing of the soil at vacuum conditions. This was evident by a small pressure rise (about 2.5×10^{-5} Torr). The primary gases released were water and hydrogen. This suggests that soil agitation at vacuum may help expedite the pump down process. However, a larger scale tilling implement would be needed to readily overturn the bed at vacuum. The single auger in these tests was insufficient to take advantage of this effect. Double tilling with at least the second tilling done in vacuum demonstrated a very uniform vertical weak soil state that provides an excellent reset of the soil for controlled test.

The effects of tamper operation were measured using the cone penetrometer. The 55 kPa, 5000 cycle/second tamper was operated at 50 percent speed for 15 to 30 s, as this was shown to compact the soil without fracturing adjacent compaction areas. A different operating point would likely be needed for a different tamper. Based on the footprint of the tamper baseplate, six tamp locations were used to encompass the bed surface with sufficient overlap. While the soil consolidation was shown to increase with the second full bin compaction, a third pass had no significant effect. There is also evidence that the pump down process alone increases the consolidation state, but stratification remains intact if there is no tilling.

The results of these tests will be used to prepare soil bins for ISRU hardware tests, including drilling, excavation, and mobility devices. Using the mitigation techniques for soil disruptions makes it possible to pre-prepare a useful soil state prior to pump down. The long pump down times can also be addressed to some degree by facility capabilities. However, means of robotic soil manipulation makes it possible to condition the soil at vacuum, and thus perform multiple tests of the hardware during the same pump down cycle. The goal had been to pull vacuum to the 10^{-6} Torr range and perform sufficient tests during a seven day period. Pending further pumping and chamber enhancements, it is more likely that 10 to 14 days are needed for a test run.

Appendix—Soil Bed Images

The following images show the soil surface throughout various stages of the vacuum process. Soil disruptions had a clear effect on the surface profile. These images were also examined to identify any smaller features changes caused by consolidation.

Test 1

Images from test 1 are shown in Figure A1. This test was done with GRC-3 soil simulant. The three images represent the soil prior to pump down (1a, 2a) and after two soil disturbance events. The top set of images was taken from camera 1, while the lower set was from camera 2 (opposite camera 1). The first soil disturbance was a ‘wave eruption’ causing a significant change in the soil surface appearance. This can be seen in the right side of image 1b. The second disturbance was a localized ‘boil’ which occurred in the already disturbed area. The result is shown in images 1c, where the disturbed area appears slightly smoother.

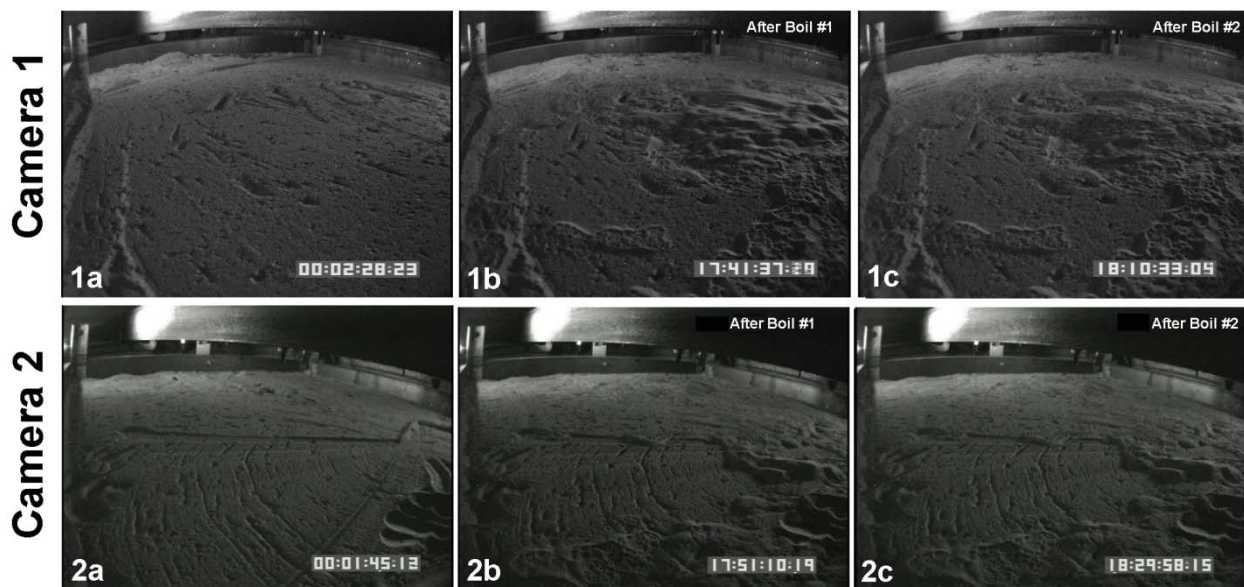


Figure A1.—Time lapse soil surface changes during Test 1.

Test 2

Figure A2 shows a series of images during test 2, all from camera 1. Pressure and time of day are labeled in each image. Image (a) was taken shortly after pump down began and shows the pre-vacuum soil state. Local boiling occurred just prior to image (b) as evidenced by the craters in the foreground of the image. A wave eruption occurred prior to image (c) in the back right. Further reduction in vacuum level (pressure alone) did not have an impact on the soil appearance, since images (d) to (f) show no significant change. Note that the cone penetrometer is shown in image (f).

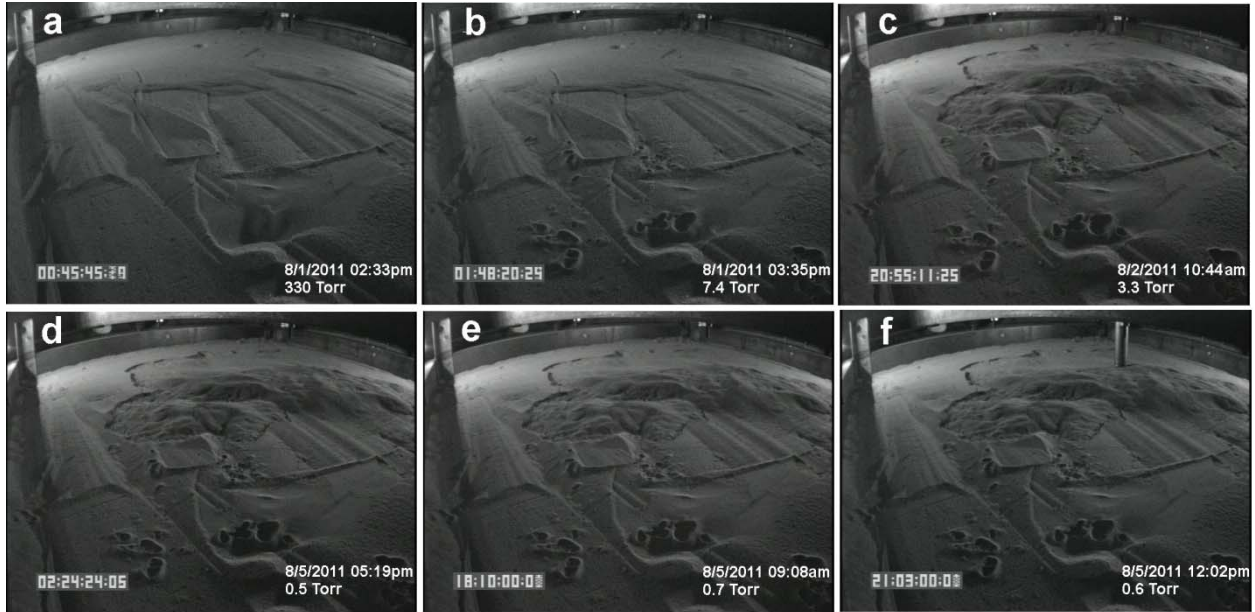


Figure A2.—Time lapse soil surface changes during Test 2.

Test 3

Three sets of images are shown in Figure A3 representing test 3. In this test, there were three camera views, each of which are shown for each time increment. The images in the first column (leftmost) were taken prior to vacuum pump down. The middle column images were taken at the lowest vacuum level, just before the cone penetration was done. The soil surface is unchanged from the pre-vacuum (1st column) images. The only soil disturbance in test 3 was localized spouting in the corners of the bin, which cannot be seen in the camera views. The final column (rightmost) images were taken after the cone penetration and after the chamber had been restored to atmospheric pressure. Again, no changes (other than the cone penetrometer hole) are visible on the soil surface.

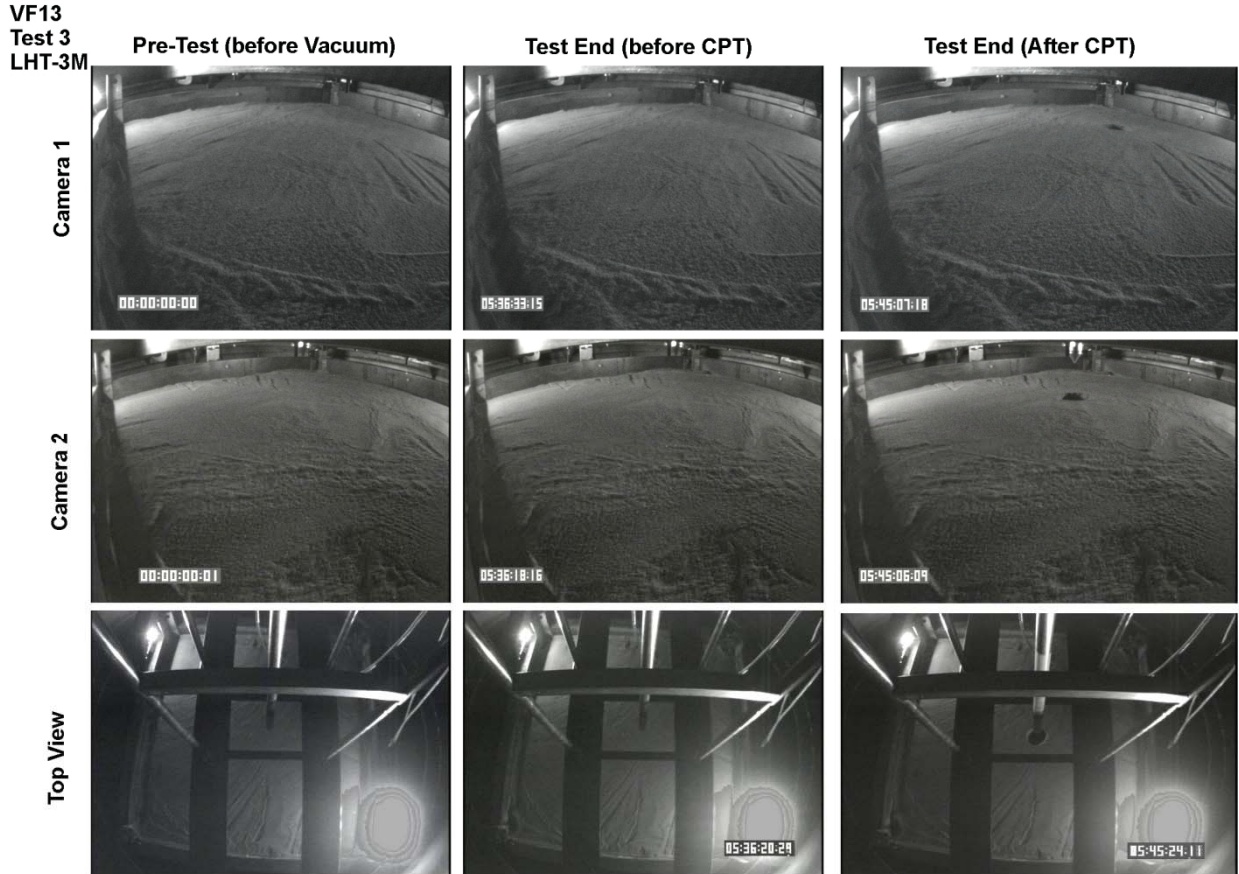


Figure A3.—Time lapse soil surface changes during Test 3.

Test 5

Two images were selected from test 5 for comparison. There were no soil eruptions. The soil was tilled during vacuum which changed the appearance of the surface. The two images below, (a) and (c), were taken in the same till state but at different pressure conditions. Image (a) was at atmospheric pressure while image (c) was at 3×10^{-3} Torr. There is only a slight change in appearance which is represented in image (b), a differencing filter of the two images. The arrow indicates the change, a ridge of a till hole had collapsed, or smoothed, at the lower pressure. This region is also shown in the close-up image (d). This is the only test in which it was noticed that a pressure alone had any visual effect on the soil surface. And even here it is not a very significant change.

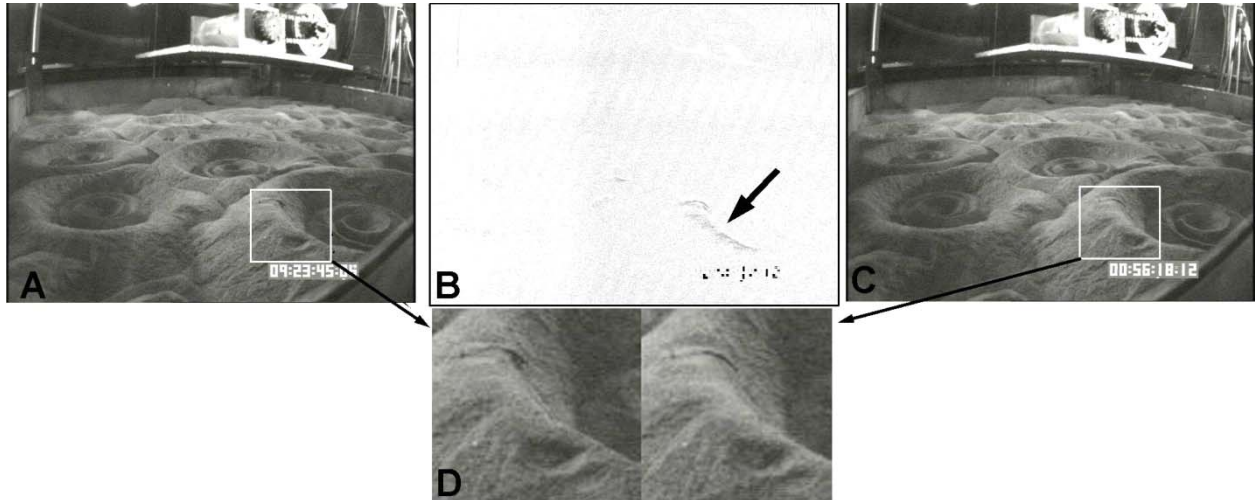


Figure A4.—Soil surface changes during Test 5.

References

1. Kennedy, K. J., et al. "NASA Human Exploration Destination Systems Roadmap - Technology Area 07", NASA. [Online] April 2010. http://www.nasa.gov/pdf/501327main_TA07-ID_rev7_NRC-wTASR.pdf
2. Perko, H.A., Nelson, J.D., and Sadeh, W.Z., "Surface Cleanliness Effect on Lunar Soil Shear Strength," *Journal of Geotechnical and Geoenvironmental Engineering*, vol. 127, iss. 4, pp. 371–383, Apr. 2001.
3. Desai, C.S., Saadatmanesh, H., and Allen, T., "Behavior of compacted lunar simulants using new vacuum triaxial device," *Journal of Aerospace Engineering*, vol. 5, iss. 4, pp. 425–441, Oct. 1992.
4. Ko, H.Y. and Sture, S., "Regolith-structure modeling," *In its Space Construction Activities (SEE N93-29108 11-18)*, iss. SEE N93-29108 11-18, pp. 31–35, Nov. 1991.
5. Halajian, J. "Soil Behavior in a Low and Ultrahigh Vacuum," in *Proc. 1964 ASME Winter Meeting*, Nov. 29-Dec. 4, 1964.
6. Stein, B.A. and Johnson, P.C. "Investigation of soil adhesion under high vacuum," in *The Lunar Surface Layer: Materials and Characteristics*, J.W. Salisbury and P.E. Glaser, Eds. New York: Academic Press, 1964, pp. 93–110.
7. Sjaastad, G. D. "An experimental study in lunar soil mechanics," in *The Lunar Surface Layer: Materials and Characteristics*, J.W. Salisbury and P.E. Glaser, Eds. New York: Academic Press, 1964, pp. 23–65.
8. Carrier III, W.D., Bromwell, L.G., and Martin, R.T., "Behavior of returned lunar soil in vacuum," *ASCE Journal of the Soil Mechanics and Foundations Division*, vol. 99, iss. SM11, Proc. Paper 10156, pp. 979–996, Nov. 1973.
9. Johnson, B.V., Roepke, W.W., and Strebis, K.C., "Shear testing of simulated lunar soil in ultrahigh vacuum," 7814, Twin Cities, MN: U. S. Bureau of Mines, 1973.
10. Grossman, J.J., Mukherjee, N.R., and Ryan, J.A., "Microphysical, microchemical, and adhesive properties of lunar material III: Gas interaction with lunar material," in *Proc. Proceedings of the Third Lunar Science Conference*, 1972, pp. 2259–2269.
11. Karafiath, L.L. and Mohr, G., "Effect of Ultrahigh Vacuum on the Friction between Metals and Granular Soil," *The Journal of Vacuum Science and Technology*, vol. 6, iss. 1, pp. 198–201, Jan. 1969.
12. Nelson, J.D. "ENVIRONMENTAL EFFECTS ON ENGINEERING PROPERTIES OF SIMULATED LUNAR SOILS," PhD thesis, Illinois Institute of Technology, Chicago, Illinois, 1967.
13. Shaw, K., "Post Test Summary Report JSC1-a Facility Assessment Testing," *NASA GRC White paper*, 2009.
14. Kleinhenz, J.E. and Wilkinson, A., 2012, "ISRU Soil Mechanics Vacuum Facility: Soil Bin Preparation and Simulant Strength Characterization," 50th Aerospace Sciences Meeting and Exhibit. American Institute for Aeronautics and Astronautics. AIAA-2012-0359.
15. He, C., Zeng, X., and Wilkinson, A., "Geotechnical Properties of GRC-3 Lunar Simulant," *ASCE J. Aerospace Eng.* 2013.26:523-534.
16. Zeng, X., He, C., and Wilkinson, A., "Geotechnical Properties of NU-LHT-2M Lunar Highland Simulant," *ASCE J. Aerospace Eng.* 2010.23: 213-218.
17. Kleinhenz, J., 2014, "Lunar Polar Environmental Testing: Regolith Simulant Conditioning," AIAA SciTech 2014: 52st Aerospace Sciences Meeting and Exhibit. American Institute for Aeronautics and Astronautics. AIAA-2014-0689.
18. LSB, Heiken, G.H., Vaniman, D.T., and French, B. M., *Lunar Sourcebook: A User's Guide to the Moon*. New York: Cambridge University Press, 1991.
19. Rohani, B. and Baladi, G.Y., "Correlation of Mobility Cone Index with Fundamental Engineering Properties of Soil," Vicksburg, MS: Army Corps of Engineers, Waterways Experiment Station, 1981.
20. Durgunoglu, T.H. and Mitchell, J.K., "Static Penetration Resistance of soils," "University of California, Berkeley, Grant Report NASA-CR-133460; SSL-SER-14-ISSUE-24, 1973.

